SIMULATING THE GLOBAL DISTRIBUTION OF $\Delta^{17}O$ IN CO_2
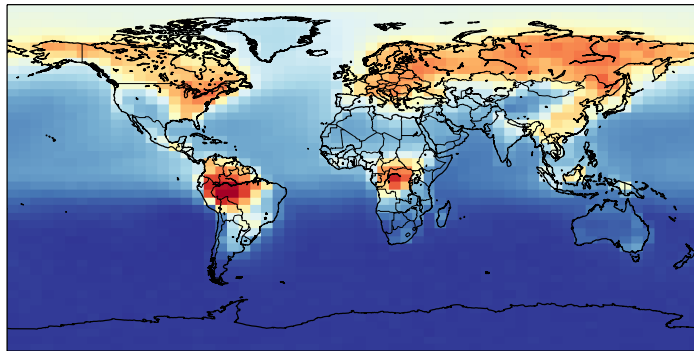
MASTER THESIS

SUBMITTED BY:
LINDA SCHNEIDER

MARCH 5, 2015

WAGENINGEN UNIVERSITY

SIMULATING THE GLOBAL DISTRIBUTION OF $\Delta^{17}O$ IN CO_2

MASTER THESIS

FOR THE STUDY PROGRAM EARTH AND ENVIRONMENT

AT THE DEPARTMENT OF

METEOROLOGY AND AIR QUALITY

AUTHOR:
LINDA SCHNEIDER

SUPERVISOR:
PROF. DR. WOUTER PETERS

MARCH 5, 2015

Abstract

The global carbon cycle plays a fundamental role in climate change. It is especially unknown yet how the biosphere, acting nowadays as a small net carbon sink, will react to changing environmental conditions and how a change in the natural carbon balance feeds back on the climate. Gross primary production (GPP), which describes the uptake of CO_2 during photosynthesis, is known to respond strongly to changing environmental conditions and it is therefore a key process to understand and quantify. The carbon and oxygen isotopes in CO_2 can help us to improve our understanding of biospheric activity. Recently the new promising tracer $\Delta^{17}O$ (excess-^{17}O) has gotten more attention. $\Delta^{17}O$ describes the deviation of ^{17}O and ^{18}O in CO_2 from a reference line and it quantifies the exchange of CO_2 between the atmosphere and the biosphere. $\Delta^{17}O$ has its origin within the stratosphere where it is positive, and is removed mostly through uptake of CO_2 by plants at the earths surface, resulting in values around 0. The abundance in the lower troposphere can thus be used as a measure for GPP. In this study, we expand the modeling of $\Delta^{17}O$ beyond the currently published box models by extending the global 3D transport model TM5. We have implemented the stratospheric source and tropospheric sinks of $\Delta^{17}O$. Our model results show lowest values of $\Delta^{17}O$ around the tropics, where GPP is high and in general low values around regions with high bioactivity. The temporal variations in $\Delta^{17}O$ follow closely the behaviour of GPP. Furthermore, we have compared the simulations to a 2-year measurement series taken in Göttingen (Germany). Although we cannot explain absolute values of the measurements with the model, the seasonal variations between the model and the measurements agree with each other. We find that the seasonality in $\Delta^{17}O$ abundances is also strongly linked to biospheric activity. For Göttingen, the impact of fossil fuel combustion and stratospheric input to the simulated abundance is low. We also use the model to study the preferred measurement strategy to estimate regional GPP from future measurements. From simulations over the Amazon Rain Forest, we conclude that a high precision (5-10 per meg) is necessary to measure seasonal and day-to-day variations in that ecosystem. We also recommend measuring not too close to the canopy to obtain representative values for the ecosystem.

Contents

Chapter 1

Introduction

Climate is important for people and people affect climate. As shown in the IPCC report, the climate on earth is changing and anthropogenic influence is evident (IPCC, 2013). The subsequent effects of changing climate will not only strike humans but also alter ecosystems, feeding back to the climate on earth. One of the main components that is studied against the background of climate change is the global carbon cycle and its feedback loops (Cox et al., 2000). The global carbon cycle is determined through sinks (such as the ocean and the biosphere) and sources (such as land-use change and fossil fuel combustion), which depend on natural and anthropogenic activities (Schimel, 1995). Whereas the identification of sinks and sources is with the current scientific knowledge comparably easy, especially the size of sinks is difficult to determine (Le Quéré et al., 2009). The difficulty to quantify sinks raises from the complexity as well as unknown processes that natural systems show. Therefore, research on significant components is fundamental to estimate their magnitude in the carbon budget.

Gross primary production (GPP) is a main component within the global carbon cycle. It is a metric for the energy fixed by plants, which can be constructed from photosynthetic activity (Woodwell and Whittaker, 1968). Due to the spatial and temporal variability of gross primary production, many studies have been conducted focusing only on net primary production (Xiao et al., 2004). This term describes the difference between gross primary production and autotrophic respiration. However, in the context of the global carbon cycle and climate change it is important to fully determine gross primary production. A possibility to do so is given by evaluating continuous measurements of CO_2 (Gilmanov et al., 2003).

CO_2 as a tracer can be used to characterize gross primary fluxes. CO_2 is removed from the atmosphere when taken up through photosynthesis and released in the course of respiration (Farquhar et al., 1993). Since CO_2 also has other sources and sinks than bioactivity, its role in gross primary production needs to be separated from other processes. In the last decades, more interest has for that reason evolved in the tracking of the stable, rare isotopes of oxygen and carbon in CO_2.

Isotopic ratios serve as a measure for CO_2 exchange between atmosphere and biosphere. Most processes in the biosphere discriminate against rare isotopes resulting in a characteristic isotope signature (Bowling et al., 2008). For instance, lighter isotopes in water are more easily evaporated or plants favor the uptake of light molecules. An isotope signature refers to the ratio of a heavy to light isotope within the sample compared to the ratio within a defined reference. For carbon, ^{12}C and ^{13}C are the

two stable isotopes. The isotopic signature $\delta^{13}C$ of a sample is

$$\delta^{13}C = \left[\frac{\left(\frac{^{13}C}{^{12}C}\right)_{sample}}{\left(\frac{^{13}C}{^{12}C}\right)_{reference}} - 1 \right] \times 1000 \qquad (1.1)$$

Whereas the heavy carbon isotope ^{13}C is often used to determine net exchange of CO_2 (Ehleringer et al., 2002), the heavy oxygen isotope ^{18}O serves as a metric to characterize gross carbon fluxes (Farquhar et al., 1993). When CO_2 comes in contact with water, the isotopic signature is changed through oxygen exchange between the H_2O and CO_2 molecules. Therefore, deriving gross primary production from ^{18}O changes requires detailed knowledge about the $\delta^{18}O$ signature in the involved water compartments. Characteristics of these water reservoirs are difficult to describe since they are connected by interaction of biological, physical and hydrological processes. For example, the $\delta^{18}O$ value of water in leafs depends among others on the plant structure, the $\delta^{18}O$ in the root zone, the temperature and the $\delta^{18}O$ of water vapor in the air (Hoag et al., 2005). Consequently, modeling $\delta^{18}O$ as a tracer for gross primary productivity is extensive. It requires a good description of many water reservoirs and their isotope signatures and thus the need for a different metric is raised.

Apart from ^{18}O, ^{17}O is an oxygen isotope, which is even less abundant within the troposphere. The isotope ratios of ^{16}O, ^{17}O and ^{18}O in CO_2 are referred to as the triple-oxygen isotope composition of CO_2. Of all CO_2 molecules 98.4 % are $^{12}C^{16}O^{16}O$, 0.07 % $^{12}C^{17}O^{16}O$ and 0.4 % $^{12}C^{18}O^{16}O$ (Eiler and Schauble, 2004). For kinetic fractionation during discrimination in physical processes, Thiemens (1999) defined the relationship between the heavy oxygen isotope ratios as

$$\delta^{17}O = \lambda \times \delta^{18}O \qquad (1.2)$$

The authors' assumption is based on a series of measurements from various terrestrial materials. The coefficient λ depends for small isotope ratios on the masses of the isotopes and can be calculated from the ratio of the reciprocal masses (Hulston and Thode, 1965). For $\delta^{17}O$ and $\delta^{18}O$ λ is 0.516. This line, which represents mass-dependent fractionation processes, is set as a reference line (RL). Deviations from this slope are given through a $\Delta^{17}O$ (called excess-^{17}O) value:

$$\Delta^{17}O = \delta^{17}O - 0.516 \times \delta^{18}O \qquad (1.3)$$

This excess is the result of mass-independent processes leading to $\Delta^{17}O \neq 0$ (Hoag et al., 2005). These mass-independent fractionation processes predominantly occur within the stratosphere, e.g. in the formation of ozone or CO_2 (Boering et al., 2004). Especially the deviation of heavy oxygen isotopes within CO_2 has become more important as a new constraint for mass-dependent processes on earth, such as biological processes.

The new tracer $\Delta^{17}O$ can be used to quantify CO_2 fluxes within the biosphere. The tracer $\Delta^{17}O$ has its origin in the stratosphere. Stratospheric CO_2 is anomalously enriched in the heavy oxygen isotopes $\delta^{17}O$ and $\delta^{18}O$ (Lämmerzahl et al., 2002). Heavy stratospheric CO_2 is formed through mass-independent reactions of non-enriched CO_2 with heavy oxygen atoms. The heavy oxygen atoms themselves are formed during photolysis of ozone (Yung et al., 1991). For stratospheric CO_2, the relation between the heavy isotopes is $\delta^{17}O \sim 2 \times \delta^{18}O$ (Wiegel et al., 2013). The excess, calculated from equation 1.3 is approximately 1‰-2‰ in the lower stratosphere (Boering et al., 2004).

Large gradients in $\Delta^{17}O$ are visible between the stratosphere and the troposphere, originating from the production of $\Delta^{17}O$ within the stratosphere and subsequent entrainment of small amounts into the troposphere towards the earth's surface. In the troposphere $\Delta^{17}O \sim 0.14‰$ (Hoag et al., 2005). The value of $\Delta^{17}O$ remains unchanged until the CO_2 comes in contact with water and undergoes equilibrium reactions. The largest water reservoirs on earth that exchange CO_2 with the air are located within the biosphere followed by the ocean (Hoag et al., 2005). Heavily enriched CO_2 is dissolved in the water and undergoes equilibrium reaction with H_2O. Thereby, the oxygen molecules of outgassing CO_2 are (partly) exchanged through lighter ones, changing the excess value. For equilibrium reactions with non-enriched H_2O, the excess is totally destroyed and thus $\Delta^{17}O$ is defined to be 0. During diffusion, kinetic fractionation takes place due to different masses of the molecules. Knowledge of both processes can be used to globally model $\Delta^{17}O$ abundances.

The global average abundance can be derived with the help of box-models. Two of these models have been presented by Hoag et al. (2005) and Hofmann (2012). Hoag et al. (2005) implemented the stratospheric source and the tropospheric sinks that alter the isotope signature of $\Delta^{17}O$ using the reference system as in equation 1.3. However, newer studies assume that equilibration of CO_2 and H_2O is the most important process to change $\Delta^{17}O$ (Hofmann et al., 2012; Barkan and Luz, 2012). Whereas kinetic fractionation depends on differences in the molecular masses of the gas, equilibration depends on the differences in the atomic masses of the isofopes (Young et al., 2002). Therefore, Hofmann (2012) has used a new reference and modification of the previous model was necessary. The new relationship between $\delta^{17}O$ and $\delta^{18}O$ is linear but in a logarithmic plot (e.g. Young et al. (2002)). The slope of the reference line λ is chosen according to the exchange coefficient of CO_2 and H_2O and has been determined through laboratory experiments (Barkan and Luz, 2012). The $\Delta^{17}O$ excess is

$$\Delta^{17}O = \ln\left(\delta^{17}O + 1\right) - 0.522 \times \ln\left(\delta^{18}O + 1\right) \tag{1.4}$$

In addition, they included more elaborate calculations for the $\Delta^{17}O$ isotope signatures. This leads to a different budget for the global $\Delta^{17}O$ abundance. Despite that the single terms can be represented in the studies from Hoag et al. (2005) and Hofmann (2012), the atmospheric distribution remains unseen. A different approach is needed to vertically and horizontally constitute the distribution of $\Delta^{17}O$.

The global distribution of $\Delta^{17}O$ can be determined using 3D models. A 3D model allows to study horizontally and vertically the mixing ratios of $\Delta^{17}O$. Combined with a high resolution, the budget of $\Delta^{17}O$ can be studied at various places. Understanding the distribution of $\Delta^{17}O$ will allow to directly quantifying gross primary production as part of the carbon cycle. The advantage of using $\Delta^{17}O$ for this purposes lays in three aspects. First, it can be used as a tracer on short and long term scales and it remains stable on its way through the troposphere towards earth (Boering et al., 2004). It means that isotopic changes will only occur at the surface. Second, $\Delta^{17}O$ is less sensitive towards the isotopic characteristics of different water pools since it is a relative measure between $\Delta^{17}O$ and $\delta^{18}O$ and therefore easier to model than isotope ratios itself (Hoag et al., 2005). Third, Hoag et al. (2005) showed that $\Delta^{17}O$ in the troposphere is predominantly determined by the stratospheric input and terrestrial bioproductivity such that isotopic modifications through other sources are relatively small.

Problem Statement
The understanding of sources and sinks of $\Delta^{17}O$ is crucial to determine gross primary production from this tracer. The global characterization of these sources and sinks can be achieved through the use of a 3D model. To make the model reliable and efficient, comparison with as many measurements

as possible needs to be performed.

The following **research questions** will be addressed in this thesis:

- What are the main gradients in $\Delta^{17}O$ when explicitly simulating its 4D distribution?

- What causes the variability in $\Delta^{17}O$ measurements taken in Göttingen between 2010-2012?

- What measurement strategy is needed to estimate regional GPP from $\Delta^{17}O$ measurements?

In Chapter 2 we describe the two box models, which have been published by Hoag et al. (2005) and Hofmann (2012). The analysis focuses on the differences between the two versions. In Chapter 3 we describe the building of the 3D modeling framework is, explain external data and the output presented for the global budget. We extend the analysis to two different ecosystems, namely the Canadian Tundra and the Amazon Rain Forest. Their responses in $\Delta^{17}O$ towards GPP is studied. In Chapter 4 we compare the model to measurements taken in Göttingen, Germany, explaining the variations in measurements. In Chapter 5 we summarize the important aspects of this thesis and use the gained knowledge to suggest a measurements strategy to estimate GPP.

Chapter 2

Current Box-Models for the global $\Delta^{17}O$ abundance

Solving the mass balance equation of $\Delta^{17}O$ allows to model its global average abundance. The motivation for modeling rises from the limited data available for tropospheric $\Delta^{17}O$ and thus the chance learn more about this tracer through modeling. The global mass balance of $\Delta^{17}O$ is defined by two main parts. First the input of CO_2 from sources with its characteristic source-dependent $\Delta^{17}O$ signature. Second the change in $\Delta^{17}O$ composition due to fractionation processes when CO_2 is exchanged. In order to predict the global average abundance in $\Delta^{17}O$ a thorough description of both the sources and the fractionations is needed.

The mass balance equation describes the change in $\Delta^{17}O$ over time by coupling the gross fluxes of CO_2 with characteristic $\Delta^{17}O$ signatures. The most challenging task is choosing representative $\Delta^{17}O$ values for the individual compartments and determining the gross primary productivity. The gross fluxes in the mass balance include terrestrial assimilation, respiration and soil invasion, ocean-atmosphere exchange, stratosphere-troposphere exchange and anthropogenic carbon emissions. Equation 2.1 shows these gross fluxes.

$$\frac{dM}{dt} = F_{AL}(t) + F_{LA}(t) + F_{resp}(t) + F_{SI}$$
$$+ F_{OA}(t) + F_{AO}(t) + F_{SA}(t) + F_{AS}(t) + F_{ff} + F_{bb} \tag{2.1}$$

with

$\frac{dM}{dt}$	rate of increase of atmospheric CO_2 [PgC/yr]
$F_{AL}(t)$	CO_2 flux atmosphere-leaf [PgC/yr]
$F_{LA}(t)$	CO_2 flux leaf-atmosphere [PgC/yr]
$F_{resp}(t)$	CO_2 emitted from terrestrial respiration [PgC/yr]
F_{SI}	soil invasion flux [PgC/yr]
$F_{OA}(t)$	CO_2 released from ocean [PgC/yr]
$F_{AO}(t)$	CO_2 taken up by the ocean [PgC/yr]
$F_{SA}(t)$	CO_2 entering the troposphere from the stratosphere [PgC/yr]
$F_{AS}(t)$	CO_2 leaving the troposphere to stratosphere [PgC/yr]
F_{ff}	CO_2 emitted from fossil fuel combustion [PgC/yr]
F_{bb}	CO_2 emitted from biomass burning [PgC/yr]

The fluxes which are noted as being time related depend on the change in tropospheric mass, whereas the others are kept constant throughout the simulations. To obtain the $\Delta^{17}O$ composition of atmospheric CO_2, we need to multiply the gross fluxes need with the corresponding isotope signatures. Equation 2.2 represents the mass balance for $\Delta^{17}O$. The product of flux and difference in isotopic compositions is called isoflux.

$$
\begin{aligned}
\frac{d\Delta_A^{17}}{dt} = \frac{1}{M_0 + \frac{dM}{dt}} \times \Big[& F_{AL}(t)\left(\Delta_{AL}^{17} - \Delta_A^{17}\right) + F_{LA}(t)\left(\Delta_{LA}^{17} - \Delta_A^{17}\right) \\
& + F_{resp}(t)\left(\Delta_{resp}^{17} - \Delta_A^{17}\right) + F_{SI}\left(\Delta_{SI}^{17} - \Delta_A^{17}\right) \\
& + F_{OA}(t)\left(\Delta_{OA}^{17} - \Delta_A^{17}\right) + F_{AO}(t)\left(\Delta_{AO}^{17} - \Delta_A^{17}\right) \\
& + F_{SA}(t)\left(\Delta_{strat}^{17} - \Delta_A^{17}\right) + F_{AS}(t)\left(\Delta_{AS}^{17} - \Delta_A^{17}\right) \\
& + F_{ff}(t)\left(\Delta_{ff}^{17} - \Delta_A^{17}\right) + F_{bb}(t)\left(\Delta_{bb}^{17} - \Delta_A^{17}\right) \Big]
\end{aligned}
\tag{2.2}
$$

with

$\frac{d\Delta_A^{17}}{dt}$	rate of increase of atmospheric Δ_A^{17}
$\frac{dM}{dt}$	rate of increase of atmospheric CO_2 [PgC/yr]
M_0	reference mass [PgC]
Δ_{AL}^{17}	$\Delta^{17}O$ value of CO_2 diffusing into leaf stomata [‰]
Δ_{LA}^{17}	$\Delta^{17}O$ value of CO_2 diffusing out of leaf stomata [‰]
Δ_{resp}^{17}	$\Delta^{17}O$ value of CO_2 emitted from soil respiration [‰]
Δ_{SI}^{17}	$\Delta^{17}O$ value of CO_2 in equilibrium with soil water [‰]
Δ_{OA}^{17}	$\Delta^{17}O$ value of CO_2 in equilibrium with ocean water [‰]
Δ_{AO}^{17}	$\Delta^{17}O$ value of CO_2 taken up by ocean [‰]
Δ_{SA}^{17}	$\Delta^{17}O$ value of CO_2 entering from the stratosphere [‰]
Δ_{AS}^{17}	$\Delta^{17}O$ value of CO_2 leaving the troposphere [‰]
Δ_{ff}^{17}	$\Delta^{17}O$ value of CO_2 emitted from fossil fuel combustion [‰]
Δ_{bb}^{17}	$\Delta^{17}O$ value of CO_2 emitted from biomass burning [‰]

The given mass balance equation has been solved in two models by Hoag et al. (2005) and Hofmann (2012). Hoag et al. (2005) presented a two box model, separating the fluxes in northern and southern hemisphere. They could for the first time show the contribution of each flux to the atmospheric value of $\Delta^{17}O$. The model from Hofmann (2012) is a one box model. The authors use it to perform a Monte-Carlo-Simulation addressing uncertainties in the budget of $\Delta^{17}O$.

The authors use different reference systems for their work. Equation 1.3 and 1.4 show the relationship for the $\Delta^{17}O$ anomaly, respectively. In the following sections we describe the two models and subsequently reproduce them to obtain a better understanding of the differences. For simplicity, we look only at the earth as a one box model and keep the original reference systems unless otherwise indicated.

2.1 Description simplified version by Hoag et al. (2005)

The simplified version is presented by Hoag et al. (2005). The authors assume the carbon budget as in 1990 with the change in mass of 3.2 PgC/yr and $M_0 = 777$ PgC/yr.

Terrestrial assimilation

Gross primary production (GPP), which is the fixation of carbon within the biosphere, is estimated to be about $100\,PgC/yr$ (Cramer et al., 1999). Hoag et al. (2005) assume that $12\,\%$ of this flux is lost due to leaf respiration (Ciais et al., 1997) and the remaining $88\,\%$ are assimilated. The assimilation is proportional to the ratio of the current mass of CO_2 $(M_0 + \frac{dM}{dt})$ and the reference mass M_0. The assimilation flux F_A is

$$F_A = 0.88 \times GPP \times \frac{M_0 + \frac{dM}{dt}}{M_0} \tag{2.3}$$

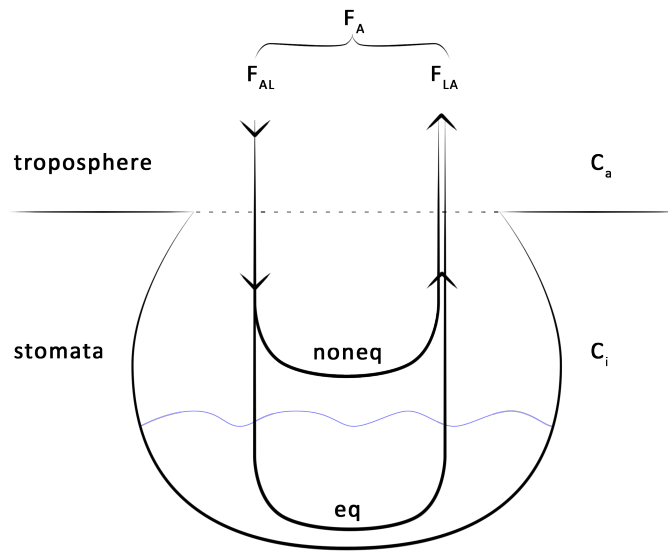Figure 2.1 shows the components that contribute to the assimilation flux.

Figure 2.1: Assimilation flux F_A: Atmosphere-leaf flux F_{AL} enters the stomata and splits into the equilibrated (eq) and non-equilibrated (noneq) part. Both leave the stomata as leaf-atmosphere F_{LA} flux. The size depends on the CO_2 concentration of the atmosphere (C_a) and the CO_2 concentration in the chloroplasts (C_i)

The flux F_A is the sum of the flux diffusing into the stomata F_{AL} and being released from the stomata to the atmosphere F_{LA}. It depends on the differences in CO_2 concentrations above the leaf (C_a) and within the leaf stomata (C_i).

$$F_{AL} = -F_A \times \frac{C_a}{C_a - C_i} \tag{2.4}$$

$$F_{LA} = F_A \times \frac{C_i}{C_a - C_i} \tag{2.5}$$

Since the amount of carbon fixed by C_3 and C_4 plants differs, the $\frac{C_i}{C_a}$-ratio is assumed to be $\frac{2}{3}$ for C_3 and $\frac{1}{3}$ for C_4 plants, respectively (Pearcy and Ehleringer, 1984). Globally, the amount of C_3 plants (f_{C3}) is about 82% and the amount of C_4 plants (f_{C4}) 18% (Still et al., 2003). Once CO_2 is within the stomata, it can exchange oxygen molecules with the available water. Therefore, part of the flux that is released from the stomata has undergone an equilibrium reaction with leaf water. Since this feeds back on the $\Delta^{17}O$ values, it is important to distinguish between the equilibrated (F_{LAeq}) and non-equilibrated ($F_{LAnoneq}$) part. The degree of equilibration is indicated through θ and 0.93 and 0.38

for C_3 and C_4 plants, respectively (Gillon and Yakir, 2000). The fluxes can be calculated according to:

$$F_{LAeq} = F_{LA} \times (f_{C3} \times \theta_{C3} + f_{C4} \times \theta_{C4}) \tag{2.6}$$

$$F_{LAnoneq} = F_{LA} \times (f_{C3} \times (1 - \theta_{C3}) + f_{C4} \times (1 - \theta_{C4})) \tag{2.7}$$

The non-equilibrated flux carries the same isotope signature as the atmosphere, since the CO_2 enters and exists the stomata without any change in isotopic ratios, making $\Delta^{17}_{LAnoneq} = \Delta^{17}_A$. The remaining CO_2 undergoes an equilibrium reaction with mass-dependently fractionated water. The signature is $\Delta^{17}_{LAnoneq} = 0$.

Respiration and Soil Invasion

Respiration from stem and root is derived from the assumption that the land stores about $2.4 \, \text{PgC/yr}$. Therefore, all assimilated carbon during photosynthesis is respired again, excluding the carbon sink.

$$F_{resp} = F_A - 2.4 \tag{2.8}$$

Hoag et al. (2005) assume that during respiration all CO_2 equilibrates with water. Thus, $\Delta^{17}_{resp} = 0$. In their model, the authors neglect soil invasion fluxes.

Stratosphere-Troposphere exchange

Differences in mass and the exchange fluxes between the stratosphere and the troposphere drive the input of $\Delta^{17}O$ into the troposphere. Hoag et al. (2005) estimate the carbon source according to Appenzeller et al. (1996) as

$$F_{SA} = 0.138 \times \left(M_0 + \frac{dM}{dt} \right) \tag{2.9}$$

In principle, the current stratospheric CO_2 mass should be taken to derive this flux. However, the time lag of 1-2 years between stratospheric and tropospheric CO_2 concentrations hardly have any effect on the results of this calculation (Hoag et al., 2005). The Δ^{17}_{SA} value is calculated from the atmospheric isotope signature and a initial stratospheric influx of $42\,‰\,\text{PgC/yr}$ (Boering et al., 2004).

$$\Delta^{17}_{SA} = 0.42 + \Delta^{17}_A \tag{2.10}$$

In the same way, the authors calculate the flux from the atmosphere to the stratosphere by reversing the sign. Since the $\Delta^{17}O$ signature of the leaving air is the same as in the atmosphere, the isoflux does not contribute to the mass balance.

Ocean flux

The carbon flux leaving the ocean is derived similar to the respiration flux. It is assumed that the net flux is $90\,\text{PgC/yr}$ and that ocean stores about $2\,\text{PgC/yr}$.

$$F_{OA} = -90 \times \frac{M_0 + \frac{dM}{dt}}{M_0} - 2 \tag{2.11}$$

The isotope signature of outgassing CO_2 is $\Delta^{17}_{OA} = 0$ since oxygen isotopes undergo equilibrium reactions with water. The flux from the atmosphere to the ocean is only the constant net flux of $90\,\text{PgC/yr}$

and the ratio of current atmospheric CO_2 mass to the reference mass. Since the air reaching the ocean comes from the atmosphere, it has the same isotopic composition as the latter one. Therefore, the isoflux is zero.

Anthropogenic fluxes

Fossil fuel combustion and land use change are the two important anthropogenic processes that alter the CO_2 concentrations within the troposphere. Hoag et al. (2005) estimate the input of fossil fuel as F_{ff}= 6 PgC/yr according to Marland et al. (2003). The $\Delta^{17}O$ signature is the same as for atmospheric O_2, namely $\Delta^{17}_{ff} = -0.155\,‰$ (Luz et al., 1999). They assume a land use change flux of $F_{bb} = 1.6$ PgC/yr (Schimel et al., 2001) with an isotope signature of $\Delta^{17}_{bb} = 0$.

2.2 Description extended version by Hofmann (2012)

Hofmann (2012) presented an extended version of the $\Delta^{17}O$ mass balance, using the reference system as in equation 1.4 and including the soil invasion flux and kinetic fractionation processes. The rate of increase in CO_2 is 4 PgC/yr and the reference CO_2 mass $M_0 = 830$ PgC/yr (Canadell et al., 2007; Le Quéré et al., 2009).

Terrestrial assimilation

The calculation of the fluxes F_{AL} and F_{LA} in the extended version is the same as in the simplified version. Only the size of input parameters varies. Hofmann (2012) assumes a GPP of 120 PgC/yr. Furthermore, the $\frac{C_i}{C_a}$ ratio is 0.7 globally and the amount of C_3 plants is 77%. All other vegetation is assumed to be C_4 plants.

In contrast to the model from Hoag et al. (2005), kinetic fractionation processes are taken into account. The CO_2 molecules entering the stomata and the ones which outgas without undergoing equilibrium are both kinetically fractionated.

$$\Delta^{17}_{AL} = \ln(\alpha_L) \times (\lambda_{kinetic} - \lambda_{RL}) \times 1000 + \Delta^{17}_A \tag{2.12}$$

$$\Delta^{17}_{LAnoneq} = \ln(\alpha_L) \times (\lambda_{kinetic} - \lambda_{RL}) \times 1000 + \Delta^{17}_A \tag{2.13}$$

The kinetic fractionation depends on $\alpha_L = 0.9926$, the kinetic fractionation factor for ^{18}O diffusing into and out of the stomata (Farquhar et al., 1993), $\lambda_{kinetic} = 0.509$ the fractionation factor for $\Delta^{17}O$ (Young et al., 2002), $\lambda_{RL} = 0.522$ the coefficient of the reference line in a $\ln(\delta^{18}O + 1)$ vs. $\ln(\delta^{17}O + 1)$ plot (see equation 1.4) and Δ^{17}_A the current isotopic composition of the atmosphere in ‰. The remaining part undergoes, in addition to kinetic fractionation, also equilibrium fractionation. During equilibrium fractionation, CO_2 exchanges oxygen isotopes with water in the leaves and thus depends on the isotope signature of leaf water Δ^{17}_L.

$$\Delta^{17}_{LAeq} = \Delta^{17}_L + \ln(\alpha_L) \times (\lambda_{kinetic} - \lambda_{RL}) \times 1000 \tag{2.14}$$

Δ^{17}_L depends on the $\Delta^{17}O$ signature found in soil water Δ^{17}_{SW}, on the amount of evapotranspiration and on the exchange of CO_2 oxygen isotopes with water within the stomata.

$$\begin{aligned}\Delta^{17}_L = &\Delta^{17}_{SW} + \ln(\alpha_{transpiration}) \times (\lambda_{RL} - \lambda_{transpiration}) \times 1000 \\ &+ \ln(\alpha_{CO_2-water}(T_{leaf})) \times (\lambda_{RL} - \theta_{CO_2-water}) \times 1000\end{aligned} \tag{2.15}$$

with $\alpha_{transpiration} = 0.9917$ (West et al., 2008) being the enrichment of ^{18}O in leaf water, $\lambda_{transpiration} = 0.522 - 0.008 \times h$, the isotope fractionation factor for transpiration in leaves and h the average humidity above the leaf. h is approximated with 80 % (Ciais et al., 1997). The last term of the equation becomes zero since λ_{RL} equals the $\Delta^{17}O$ equilibrium fractionation factor. The $\Delta^{17}O$ signature in soil water is calculated under the assumption that the isotope signature of the water in the root zones falls on the global meteoric water line (GMWL) (Luz and Barkan, 2010).

$$\Delta^{17}_{SW} = (\lambda_{GMWL} - \lambda_{RL}) \times \ln(\delta_{SW} + 1) \times 1000 + \gamma_{GMWL} \tag{2.16}$$

The GMWL has a slope of $\lambda_{GMWL} = 0.528$ and an intercept of $\gamma_{GMWL} = 0.033\%o$. $\delta_{SW} = -7.5\%o$ represents the $\delta^{18}O$ isotope signature of soil water (Ciais et al., 1997). These values lead to an isotopic composition of soil water of $\Delta^{17}_{SW} = -0.01\%o$. The isotope signature for leaf water is then $\Delta^{17}_L = -0.07\%o$

Respiration and Soil Invasion

The authors calculate respiration, assuming that the biosphere acts as a carbon sink. The net sink is 3 PgC/yr (Canadell et al., 2007; Le Quéré et al., 2009) .

$$F_{resp} = F_A - 3\,\text{PgC/yr} \tag{2.17}$$

$$= 0.88 \times \text{GPP} \times \frac{M_0 + \frac{dM}{dt}}{M_0} - 3 \tag{2.18}$$

The respired CO_2 undergoes equilibrium processes with soil water and is in addition subject to kinetic fractionation when diffusing into the atmosphere.

$$\Delta^{17}_{resp} = \Delta^{17}_{SW} - (\lambda_{RL} - \theta_{CO_2-water} \times \ln(\alpha_{CO_2-water}(T_{soil})) - \ln(\alpha_s) \times (\lambda_{kinetic} - \lambda_{RL}) \times 1000 \tag{2.19}$$

with the $\delta^{18}O$ kinetic fractionation factor in and out of soils, $\alpha_s = 0.9928$. Since the equilibrium fractionation factor θ for CO_2 water exchange of $\delta^{18}O$ is the same as the slope of the reference line λ, the middle term does not contribute to the equation.
Next to the respiration flux, Hofmann (2012) takes the soil invasion flux into account.

$$\Delta^{17}_{SI} = \Delta^{17}_{SW} - (\lambda_{RL} - \theta_{CO_2-water} \times \ln(\alpha_{CO_2-water}(T_{soil})) \times 1000 \tag{2.20}$$

The flux describes the CO_2 which diffuses into the upper soil layer and equilibrates with the present soil water. The soil invasion flux is approximated with $F_{SI} = 30\,\text{PgC/yr}$ (Stern et al., 2001). The isotopic composition depends on the isotope signature of soil water and the equilibration factor. The latter being zero again.

Stratosphere-Troposphere exchange

The stratosphere-troposphere flux is derived from Appenzeller et al. (1996) and is 100 PgC/yr. It is analogue to the simplified version dependent on the mass of CO_2 within the atmosphere.

$$F_{SA} = 100 \times \frac{M_0 + \frac{dM}{dt}}{M_0} \tag{2.21}$$

The isotopic composition of stratospheric air is in the reference system with $\lambda_{RL} = 0.522$, $44.5\,‰$ PgC/yr (Boering et al., 2004). From the assumption that 100 PgC/yr enters the troposphere, the Δ^{17}O value Δ^{17}_{strat} can be derived.

$$\Delta^{17}_{strat} = \Delta^{17}_{A} + 0.445 \tag{2.22}$$

The flux leaving the troposphere F_{AS} is the reverse of the entering amount. But since the isotopic signature of Δ^{17}O is the same as for atmospheric CO_2, the isoflux of troposphere-stratosphere exchange is 0.

Ocean flux

The ocean-atmosphere flux F_{OA} is estimated as in Hoag et al. (2005) and 90 PgC/yr. The CO_2 reaching the sea surface equilibrates with the ocean water.

$$\Delta^{17}O = \Delta^{17}_{ocean} - (\lambda_{RL} - \theta_{CO_2-water}) \times \ln(\alpha_{CO_2-water}(T_{ocean})) \times 1000 \tag{2.23}$$

Ocean water itself has an isotopic composition of $\Delta^{17}_{ocean} = -0.005‰$ (Luz and Barkan, 2010). As the equilibrium fractionation factor θ for CO_2-water is the same as the slope λ for the reference line RL, the last term becomes again zero. The isoflux from the atmosphere to the ocean is, as described by Hoag et al. (2005), not contributing to the mass balance and thus 0.

Antropogenic fluxes

Hofmann (2012) defines the fossil fuel emissions as $F_{ff} = 8$ PgC/yr (Canadell et al., 2007; Le Quéré et al., 2009). This is considerably higher than in the other model. The authors take increasing fossil fuel emissions world wide since the beginning of the 21st century into account. The carbon biomass burning flux, as the most dominant change of land use, is $F_{bb} = 1$ PgC/yr (Canadell et al., 2007; Le Quéré et al., 2009; van der Werf et al., 2004). The isotopic composition of the fossil fuel combustion processes is taken from a study by Horváth et al. (2012) looking at high temperature combustion and car exhaust, which has a signature of $\Delta^{17}_{ff} = -0.32‰$. However, for low temperature combustion as it occurs during biomass burning, the effect of equilibration with water contributes to the isotope signature and therefore $\Delta^{17}_{bb} = -0.21‰$ (Horváth et al., 2012).

2.3 Comparison

The reproduced versions of the models from Hoag et al. (2005) and Hofmann (2012) indicate that the two box models determine different isofluxes, which feeds back on the global mass balance. Appendix A.1 gives an overview of the used parameters. Figure 2.2 shows the yearly global Δ^{17}O values for both models after the start of the model runs.

Both models reach a steady state after 10 years. The steady state value is approximately $0.1‰$ and $0.06‰$, respectively. These values are in agreement with measurements of tropospheric Δ^{17}O by Thiemens et al. (2014). Thiemens et al. (2014) presented a timeseries of tropospheric Δ^{17}O from 1991-1999 measured at La Jolla, California, USA. For the same reference system as here, the authors show a steady state value of $0.08 \pm 0.04‰$. The steady state value for Hoag et al. (2005) in their original reference system would be $0.14‰$.
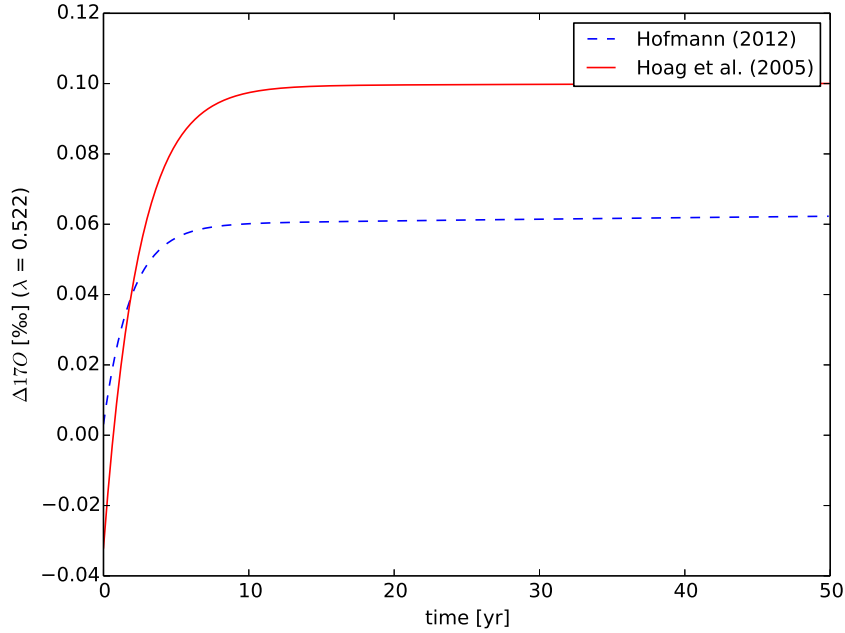
Figure 2.2: Global isotope signature $\Delta^{17}O$ in ‰. The red solid line represents the outcome from Hoag et al. (2005), the blue dashed line from Hofmann (2012). Note that the outcome from Hoag et al. (2005) was converted to the same reference system as Hofmann (2012) uses: The $\delta^{17}O$ value is calculated with equation 1.3 and inserted into equation 1.4. $\Delta^{17}O$ is calculated assuming that $\delta^{18}O$ is globally 41.5‰ for both models (Francey and Tans, 1987).

The differences in global means are due to disagreement on the size of the isofluxes between the two models. Figure 2.3 shows the isoflux budgets for both models. Deviations between the isofluxes can be mainly found in these terms: The atmosphere-leaf isoflux, the respiration isoflux and the equilibrated and non-equilibrated leaf-atmosphere isoflux.

The inclusion of kinetic fractionation is, among the size of GPP, responsible for the different patterns in isofluxes between the models. Hofmann (2012) assumes that CO_2 diffusing into and out of reservoirs undergoes kinetic fractionation, changing $\Delta^{17}O$. Hoag et al. (2005) neglect this process. The atmosphere-leaf flux is therefore highly negative, as predominantly light molecules enter the stomata, leaving relatively more ^{18}O than ^{17}O in the surrounding air. The non-equilibrated leaf-atmosphere flux is however positive, since the CO_2 again undergoes kinetic fractionation when diffusing out of the stomata.

The small differences in the ocean-atmosphere, fossil fuel and biomass burning isofluxes come from differences in isotope signatures. However, the total differences between Hoag et al. (2005) and Hofmann (2012) in these isofluxes is little.

Slight variations in isofluxes between the models are due to the use of the different reference systems. The conversion into the same reference system would require the knowledge of $\delta^{18}O$ ratios of the reservoirs. Since only a global value for $\delta^{18}O$ is available, it is only possible to derive the global $\Delta^{17}O$ abundance for the same reference system. For the individual processes $\delta^{18}O$ is not available and we keep the reference systems as in their original study.
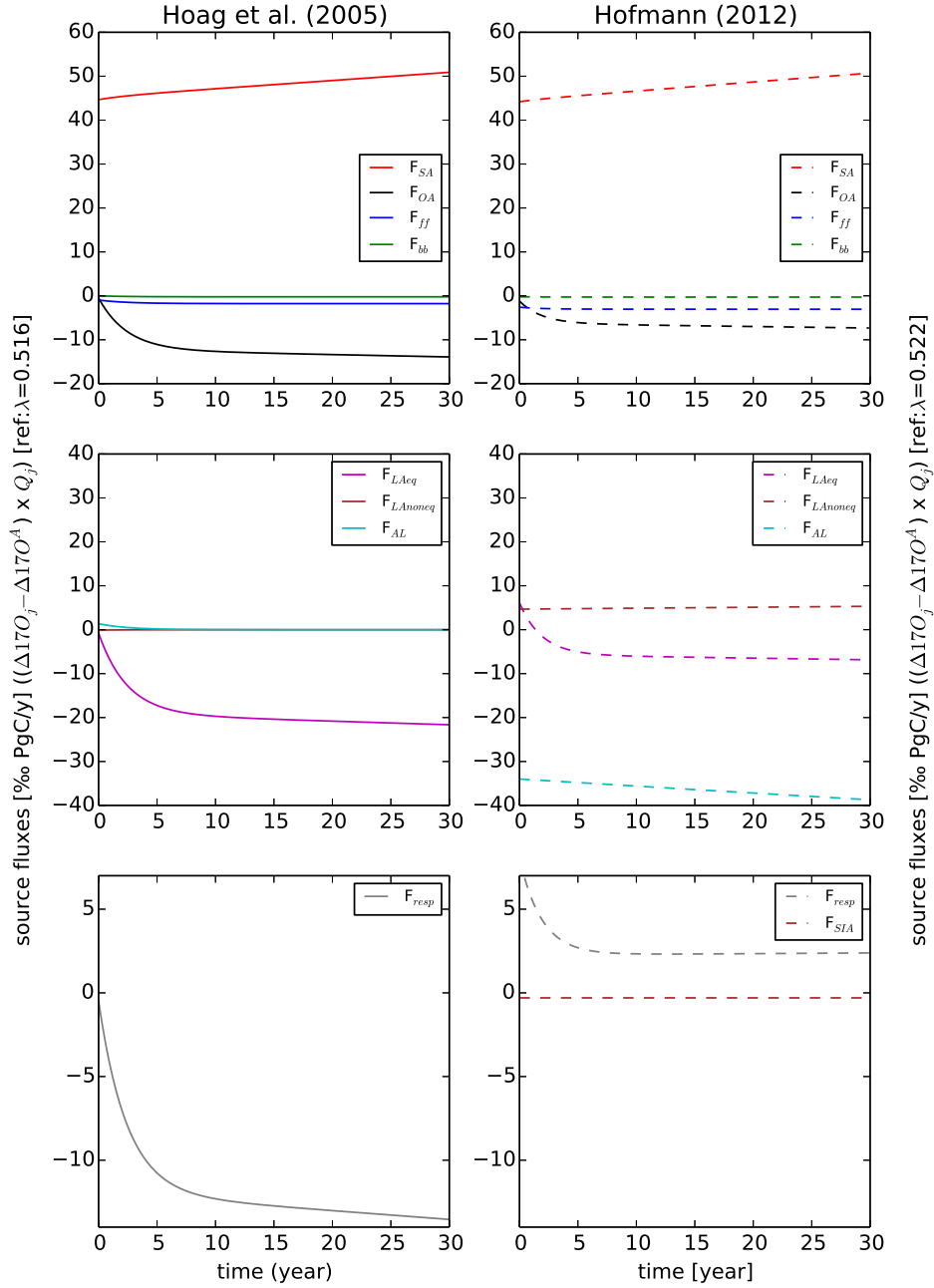
Figure 2.3: Modelled isofluxes in ‰ PgC/yr during a 30 year time period. The left graphs are derived according to Hoag et al. (2005) and the right ones according to Hofmann (2012). SA = stratosphere-atmosphere isoflux, OA = ocean-atmosphere isoflux, FF = fossil fuel isoflux, bb = biomass burning isoflux, LAeq = equilibrated leaf-atmosphere isoflux, LAnoneq= non-equilibrated leaf-atmosphere isoflux, AL = atmosphere-leaf isoflux, resp = respiration isoflux, SIA = soil invasion isoflux

One of the uncertain fluxes on earth is GPP (Beer et al., 2010). Since it determines several isofluxes, the global abundance of $\Delta^{17}O$ is expected to change if varying GPP. Figure 2.4 shows the sensitivity of the two models towards changing GPP.
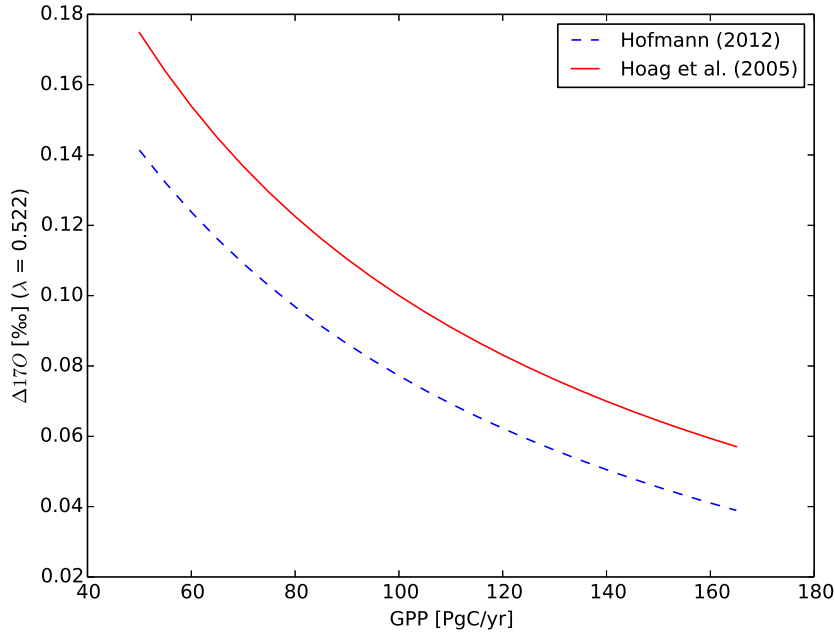

Figure 2.4: Global values of $\Delta^{17}O$ depending on GPP. The red solid line represents the outcome from Hoag et al. (2005), the blue dashed line from Hofmann (2012). The values represent the timestep t=30 years. The outcome from Hoag et al. (2005) was converted to the same reference system as Hofmann (2012): The $\delta^{17}O$ value is calculated with equation 1.3 and inserted into equation 1.4. $\Delta^{17}O$ is calculated assuming that $\delta^{18}O$ is globally 41.5‰ for both models (Francey and Tans, 1987).

Changing GPP from 50 PgC/yr to 150 PgC/yr leads to a decrease in $\Delta^{17}O$ of about -0.09‰ for the model from Hofmann (2012) and -0.11‰ for the model from Hoag et al. (2005). The results indicate that depending on the size of global GPP, the $\Delta^{17}O$ abundance is affected a lot.

2.4 Discussion

The difference between the two models lays within the use of the reference system as well as the way they include fractionation. In absolute means, the choice of the reference system reduces the global $\Delta^{17}O$ value from Hoag et al. (2005) about 0.04‰. The difference between the models is after conversion into the same reference system 0.04‰, indicating that both effects are evenly important.

The difference in the global abundance of $\Delta^{17}O$ suggests that also local differences are likely. This hypothesis is strengthened by two facts. First, the isofluxes that determine the mass balance differ between the two models. Since the isofluxes depend on local characteristics, such as surface cover and climate conditions, it is very probable that the two models would differ between their local $\Delta^{17}O$ abundances. Second, large variations in GPP alter the global $\Delta^{17}O$ abundance. Since GPP is locally variable, $\Delta^{17}O$ we also expect it to vary locally.

Alternation in the global abundance of $\Delta^{17}O$ arise from different origins. As it is shown in a literature review by Hofmann (2012), uncertainties exist in GPP, the respiration flux, the stratosphere-influx, the soil invasion flux and the global distribution of C_3 and C_4 plants. Both authors therefore tested their models against uncertainties. As a result, it can be concluded that the models react differently towards variations in the named parameters. Hoag et al. (2005) performed a sensitivity study showing that the terrestrial gross fluxes and the stratosphere-troposphere influx have the most effect on the global budget. Therefore, they concluded that changes in $\Delta^{17}O$ are to the biggest extend due to variations in GPP and that $\Delta^{17}O$ is thus a new constraint for GPP. Hofmann (2012) in return, showed in a Monte-Carlo simulation that next to GPP, the distribution of plant species, the stratosphere-troposphere influx and soil invasion largely determine the global $\Delta^{17}O$ abundance. Therefore, they have recommended to look in more detail at the budget in order to strengthen the use of $\Delta^{17}O$ as a new constraint for GPP.

For further investigation it is necessary to show spatial and temporal patterns. Modeling the isofluxes at higher resolutions allows to investigate the budget in more detail. The results can give indications on the $\Delta^{17}O$ abundance for different regions and also the impact of flux uncertainties on local $\Delta^{17}O$ abundances. Consequently, the next step is to set up a high resolution 3D model that allows to study the budget of $\Delta^{17}O$. In the next chapter we present the implementation of sinks and sources of $\Delta^{17}O$ in the 3D atmospheric transport model TM5 according to the present box-models.

Chapter 3

3D Transport Model

3D models enable to study horizontal and spatial patterns of quantities. The transport model TM5 allows to resolute chemical tracers spatially on a three dimensional scale (Huijnen et al., 2010) as well as in time. Unique about this model is the ability to simulate on high resolutions by applying a two-way nested zooming algorithm. Global parent grids are defined on a resolution of $6° \times 4°$ (longitude $\times$ latitude) and boundary conditions can be passed on from the coarse to the zoomed (child) region and vice versa. This allows to locally simulate up to a resolution of $1° \times 1°$ (Krol et al., 2005).

Local conditions within the gridboxes are characterized through the use of offline input data, such as meteorological data to represent weather and surface conditions of land and ocean. The meteorological data used comes from the ERA interim reanalysis data from the European Center for Medium Range Weather Forecast (ECMWF). The coherent and complete dataset of global atmospheric circulation is obtained by performing a multivariate reanalysis of 3-hourly surface and 6-hourly upper air parameters. The gained data has to match observations and serve the law of physics. Data assimilation is done using the ECMWF operational forecasting system from 2006-2007 to extrapolate local observations to nearby locations (Dee et al., 2011).

The transport of tracers in TM5 is calculated with the help of an operator splitting algorithm. This means that processes are calculated individually for the time step $\Delta t/2$ and subsequently the operations are repeated in reversed order. TM5 distinguishes between four relevant processes: Horizontal (XY) and vertical (Z) advection, vertical mixing (V), and chemistry (C). The processes are performed in the named order and backwards (Krol et al., 2005).

- **Advection** characterizes transport horizontally with the mean wind. The algorithm is solved with a slope scheme, including a mean concentration for each grid box and a gradient within this volume. Description of the advection algorithm can be found in Russell and Lerner (1981).

- **Vertical Mixing** includes deep convection and vertical diffusion due to heating of the surface (Huijnen et al., 2010). Convection fields are taken directly from ECMWF and the vertical diffusion is derived from two different schemes, separately for the free-troposphere (Louis, 1979) and boundary layer (Holtslag and Boville, 1993). This allows to take stable conditions in the Atmospheric Boundary Layer into account.

- **Sources and Sinks** describe emissions, boundary conditions of the stratosphere and wet deposition. This includes mole fractions of stratospheric long-living gasses from satellite measurements, weather data for precipitation and emissions from different inventories (Huijnen et al., 2010).

- **Chemistry** includes gas and aqueous phase reactions as well as photolysis (Huijnen et al., 2010). It is optional to use in TM5, and not applied in this work.

In this work we use a horizontal domain size of $6° \times 4°$ (longitude $\times$ latitude). In the vertical domain 25 levels are present, defined through hybrid sigma-pressure coordinates. This allows to take the local terrain into account by making the levels over one point equidistant. The time step is set to $\Delta t = 1.5$ hours.

We implement sources and sinks of $C^{16}O^{16}O$, $C^{16}O^{17}O$ and $C^{16}O^{18}O$ into TM5 as three individual tracers. The studies of Hoag et al. (2005) and Hofmann (2012), which are described in chapter 2, serve as a base. The study of Hofmann (2012) is modified by replacing the exchange coefficient $\theta_{CO_2-water}$ with 0.5229. The research of Barkan and Luz (2012) names this number as a result of measurement improvements. The study of Hoag et al. (2005) is re-applied as before.

To fully explore the potential of a 3D model, we replace global fluxes for assimilation, respiration, fossil fuel emissions, biomass burning and atmosphere-ocean exchange with local values by means of offline data. This assures to take spatial and temporal variations into account. The carbon tracers $C^{16}O^{16}O$, $C^{16}O^{17}O$ and $C^{16}O^{18}O$ are simulated and their mole fractions recorded. They are offline processed into $\Delta^{17}O$ values. Furthermore, isofluxes are calculated for every grid box individually and summed to obtain global values. The offline data, which we use, is described in the following section.

3.1 Methods

Biosphere

Carbon fluxes come from simulations with the combined model SiBCASA. The Simple Biosphere (SiB) model presents biophysical processes and the Carnegie-Ames-Stanford Approach model (CASA) holds biogeochemical processes (Schaefer et al., 2008). The combined model SiBCASA enables to calculate the water, energy and carbon budget on scales of 10 minutes and a resolution of $1° \times 1°$, by accessing current state meteorological data from ECMWF (van der Velde et al., 2013). SiBCASA calculates the carbon flows by defining different pools and estimating the loss and gains depending on other pools as well as respiration and disturbances. It represents local conditions as detailed as possible by assigning biome types to observed vegetation cover. To simulate the exchange of CO_2 within the biosphere, SiBCASA has an integrated stomatal conductance model, a C_3 enzyme kinetic model and a C_4 photosynthesis model (van der Velde et al., 2013). Consequently gross primary productivity can be derived separately for C_3 and C_4 plants. In this study, monthly mean data for respiration, gross primary productivity and internal and atmospheric CO_2 mole fractions from SiBCASA are used as input for TM5.

Respiration is calculated online in TM5 according to the Q-10 relationship, which indicates the change in respiration by a 10 K change in temperature (Potter et al., 1993).

$$\text{Respiration} = R_0 \times Q_{10}^{\frac{T_1-T_0}{10}} \tag{3.1}$$

The temperature T_1 represents the 2 m air temperature from the ECMWF database. Usually, equation 3.1 would require soil temperature as an input value for T_1, which is lower than air temperature. Soil temperature is however less frequently available than air temperature from ECMWF. Therefore the parameter R_0, which is derived from SiBCASA for a reference temperature of $T_0 = 273.5$ K, also includes a scaling factor. Equation 3.1 allows to simulate a daily cycle for respiration by using daily temperature values. Q_{10} is set to 1.5.

The respiration is globally 129 PgC/yr for the year 2011 and its distribution according to the same pattern as for gross primary productivity (figure 3.1). This number is larger than values around 100 PgC/yr from a large collection of soil respiration data from all around the world (Bond-Lamberty and Thomson, 2010).

We take gross primary productivity directly from SiBCASA output. Figure 3.1 shows the global distribution of GPP. Total GPP globally is 133 PgC/yr for the year 2011, with the main source in the tropics. The average number as well as the observed pattern of high bioactivity in the warm regions where light and water are hardly limited are in accordance with literature (Beer et al., 2010).
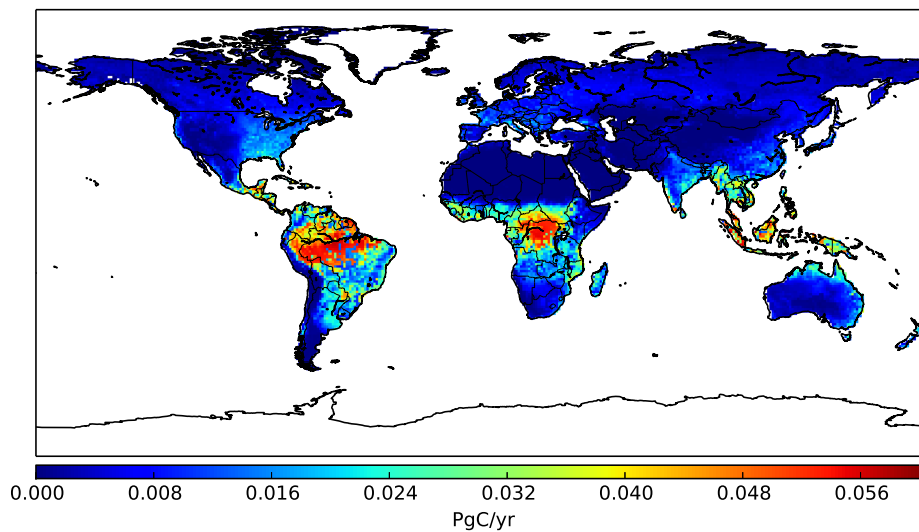
Figure 3.1: Gross Primary Productivity for the year 2011 from the SiBCASA model. High uptake of CO_2 occurs around the tropics.

Next to the spatial pattern, the biosphere shows temporal variations. Figure 3.2 shows global respiration and gross primary production in 2011, peaking both within the summer months of the northern hemisphere. At that time the large amount of vegetation, present in the northern hemisphere, is most active assimilating and respiring carbon. The large difference between the two curves is due to high emissions of biomass burning, which enhance CO_2 outgassing.

We take internal (C_i) and atmospheric (C_a) CO_2 concentrations from SiBCASA and weighted them according to GPP. The results of monthly C_i and C_a values thus represent conditions as present during activity of high photosynthesis. The global values for $\frac{C_i}{C_a}$ range from 0.2 to 0.98 as shown in figure 3.3. The range is thereby larger than reported for C_3 (0.66) and C_4 (0.33) plants (Pearcy and Ehleringer, 1984). The global mean is 0.73, which is in accordance with literature from Ciais et al. (1997).
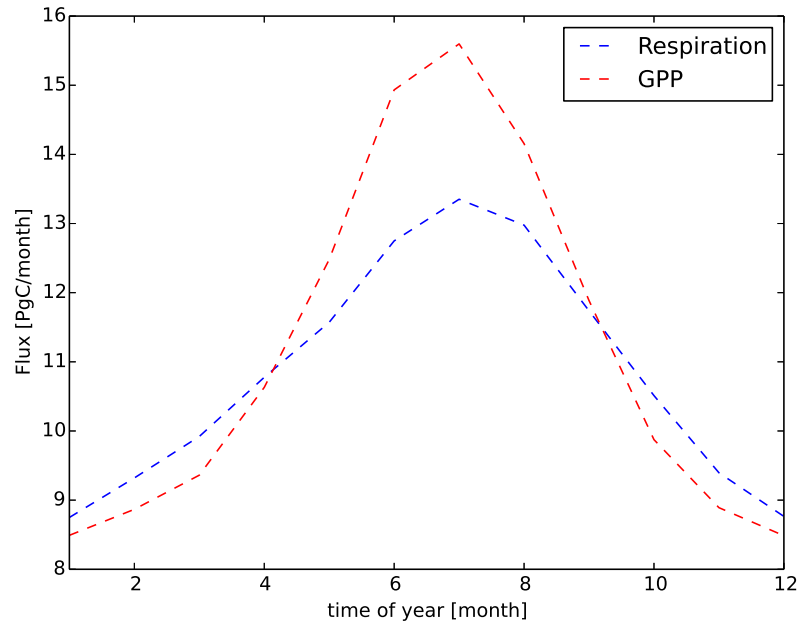
Figure 3.2: Global respiration (blue) and global gross primary productivity (red) in PgC/month for the year 2011.
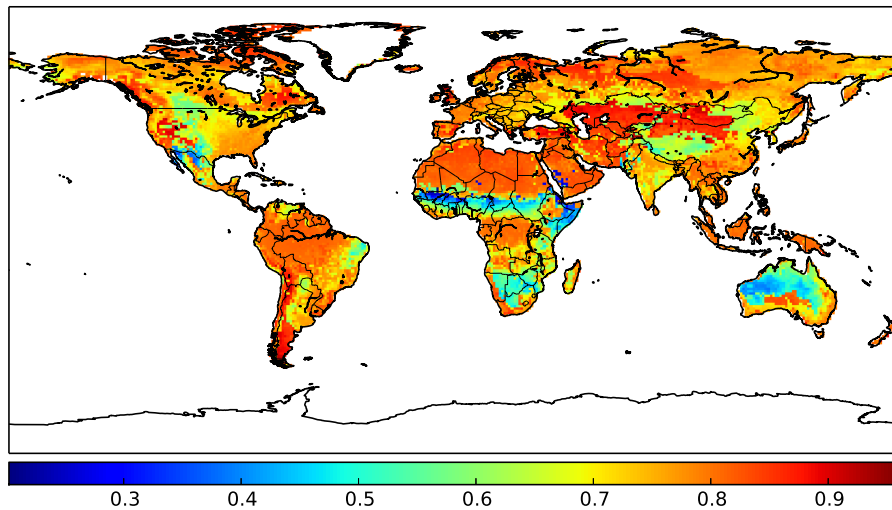

Figure 3.3: ci/ca ratios for the year 2011 from the SiBCASA model

Values are high in regions where snow cover is present and if they were larger than 1, we manually set them to 0.98. Since CO_2 uptake is very little during times of snow cover, SiBCASA provides very uncertain results, leading to fractions larger than 1. As values of $\frac{C_i}{C_a}$ ratios are multiplied with gross primary productivity, which is low too during these periods, the effect of high ratios will be negligible. The manual modification of values larger than 1 is thus appropriate. In regions around the

equator, where many C_4 plants are available values drop down to 0.2. The higher reported values of 0.3 in literature are usually derived under laboratory settings for distinct species, whereas SiBCASA accounts for the processes that are known to occur. The C_i concentrations are influenced i.e. not only by stomatal conductance and enzyme activity but likewise environmental conditions such as leaf to air water vapour pressure (Bunce, 2005). These meteorological conditions are also part of the calculations in SiBCASA.

Fossil fuel

We take fossil fuel data from the GEOCARBON project. The fluxes are based on emissions from the EDGAR 4.2 database, coupled to country and sector specific time profiles by the Institute for Energy Economics and the Rational Use of Energy (IER) in Stuttgart, Germany, as part of the CARBONES project. Highest fossil fuel emissions occur in regions with high economic activity such as Europe, China and North America (see Appendix A.2, figure 1).

Biomass burning

Biomass burning is one form of land use change. SiBCASA calculates emissions of carbon fluxes from this source by using burned area estimated on a 0.25° resolution from the Global Fire Emissions Database version 4 (GFED4) (Giglio et al., 2013), maps of vegetation types and an estimate of the combustion completeness. Estimates of the burned area in the GFED4 database are derived from satellite measurements (Moderate Resolution Imaging Spectroradiometer (MODIS)) of fire counts, active fire data from the Tropical Rainfall Measuring Mission, Visible and Infrared Scanner (VIRS) and the Along-Track Scanning Radiometer (ATSR) (van der Werf et al., 2010). Biomass burning is mostly present in the tropics (see Appendix A.2, figure 2).

Soil Invasion

Soil Invasion can differ within one order of magnitude (Hofmann, 2012). Because of this uncertainty and a lack of offline data, we choose that soil invasion is 30 % of respiration. This is the same ratio as applied in Hofmann (2012).

Ocean

We calculate the exchange of CO_2 between ocean and atmosphere from the difference in partial pressure and meteorological variables. Next to concentration gradients between the two media, the wind speed and parameters that characterize the surface turbulence are determining the CO_2 fluxes (Wanninkhof 1992). With the empirical relationship in equation 3.2 the gas transfer velocity is calculated. u_{av} is the average wind speed and Sc the Schmidt-number, a ratio of viscosity to mass diffusivity.

$$k = 0.31 \times \frac{u_{av}^2}{\sqrt{\frac{Sc}{660}}} \qquad (3.2)$$

The CO_2 flux is subsequently calculated as

$$F_O = k \times s \times pCO_2 \qquad (3.3)$$

where s is the solubility and pCO_2 the difference in partial pressure. The formula gives values for either uptake (negative) or release (positive) of CO_2. Thus in the model, isofluxes were calculated by applying isotope signatures of either the ocean water or the atmosphere, depending on the netflux for that grid box. Furthermore, in areas covered with sea ice the flux was set to 0. We take data for wind speed and sea ice from ECMWF, the Schmidt number, partial pressure and solubility come from

inverse estimates by Jacobson et al. (2007).

Stratosphere

To implement the stratosphere as source for $\Delta^{17}O$ we apply its isotope signature ($\sim 0.6\,‰$ in the lower stratosphere) (Boering et al., 2004) to the mass of CO_2 in the top 5 levels (20 km-50 km) for every grid box. We choose this approach since TM5 calculates transport of mass within and across grid boxes and uses ECMWF data to describe the stratosphere-troposphere exchange, making this flux a predefined component of TM5. This approach however, leads to very small values for $\Delta^{17}O$ at the surface. Since the $\Delta^{17}O$ abundance at the surface was for both versions (Hoag et al., 2005; Hofmann, 2012), about the same factor too low we decided to set the isotope signature for the 5 top levels to $2.76\,‰$. The result is a good agreement between the mean abundance of $\Delta^{17}O$ at the surface and the box models. An overview of isotopic measurements in the stratosphere by Wiegel et al. (2013) indicates that enrichment of ^{17}O in CO_2 varies with height, season and altitude. Results from a flight experiment present values of $\Delta^{17}O$ up to $5\,‰$ for heights until 20 km (Boering et al., 2004). Since the top 5 levels, to which the isotope signature is assigned, spread over a large vertical distance, the assumption to increase the isotope signature is reasonable.

3.2 Results

Global mole fractions of CO_2, as output of TM5, indicate the correctness of parametrizations, and implementation and are shown in figure 3.4. The figure is obtained by initializing the model with CO_2 mole fractions for every grid box from the carbontracker database from 27.12.2008. This leads to an initial global mole fraction of 388 ppmv. Then separate runs are performed for each of the source/sink terms and all together (global). Global abundances increase about 5 PgC/yr, following the strong seasonal cycle from the biosphere. The mole fractions for fossil fuel combustion, biomass burning and ocean uptake are according to expectation of the external data. The net uptake from biosphere is rather small because SiBCASA assumes a steady state for net ecosystem exchange. Fluxes from the carbontracker database would lead to different results.

The average global abundance of $\Delta^{17}O$ at the surface between 2010-2013 is $0.14\,‰ \pm 0.02\,‰$ (1σ standard deviation, n=974) for Hoag et al. (2005) and $0.08\,‰ \pm 0.02\,‰$ for Hofmann (2012) (1σ standard deviation, n=974). The mean values for Hoag et al. (2005) are $0.12\,‰ \pm 0.01\,‰$ for the northern and $0.15\,‰ \pm 0.01\,‰$ for the southern hemisphere, respectively. These numbers are in accordance with the box models. Figure 3.5 shows the average distribution averaged over the bottom 1 km for the years 2010-2012 for both models, respectively. Although different in absolute abundances, both results show similar spatial patterns.

- Regions with high bioactivity show the lowest values for the excess due to large carbon exchange and isotope discrimination during equilibration and kinetic fractionation

- The air over northern hemispheric oceans is depleted in $\Delta^{17}O$ compared to the southern. The pattern is a result of large land areas where bioactivity is likewise large. Due to fast hemispheric transport times, signals of large CO_2 uptake can still be seen over the ocean, especially in the lowest vertical levels

- The spread in the southern hemisphere is larger than in the northern. The almost exclusive processes altering $\Delta^{17}O$ in the southern half are equilibration with the ocean (small amount
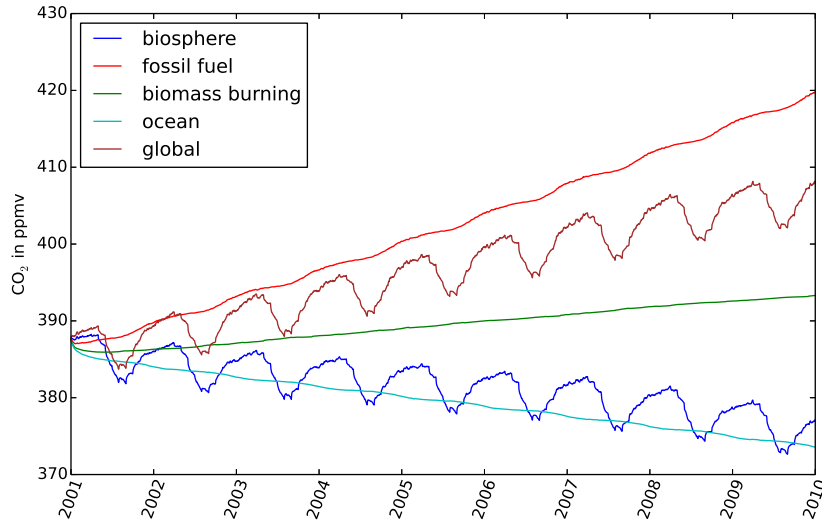
Figure 3.4: The different contributors to the globally simulated CO_2 mole fractions: biosphere, fossil fuel emissions, biomass burning and ocean

but large area) and uptake from the biosphere (large amount but small area). In the northern hemisphere, bioactivity is for individual grid boxes lower than in the southern hemisphere, leading to a smaller spread. Slow inter-hemispheric transport dampens mixing of surface-air between the two sides, leading to a sharp transition

Isofluxes in each grid box mainly determine the value of $\Delta^{17}O$ within that area. Figure 3.6 shows the isofluxes. Stratospheric input and exchange of CO_2 with the biosphere determine the global balance of $\Delta^{17}O$. Assimilation is for both models negative, however due to inclusion of kinetic fractionation, the leaf-atmosphere fluxes are positive for the model from Hofmann (2012). The same reason holds for the difference in respiration. Fossil fuel combustion, biomass burning and carbon exchange with the ocean contribute only little.

Compared to the box models, the stratosphere contributes yearly about $10\,\text{‰}PgC$ less in the simulations with TM5. This effect is compensated by a smaller change in $\Delta^{17}O$ through out gassing from the ocean. The differences in all biospheric isofluxes from TM5 to the isofluxes derived from the box models are due to two reasons, named in the order of importance: (1) Isofluxes are in TM5 obtained for every grid box and then summed. Calculations of global carbon fluxes with average global $\Delta^{17}O$ values would have led to almost equal isofluxes as in the box models. (2) We use slightly different carbon fluxes for the biosphere.

The new modeling framework allows to further zoom in spatially and temporarily. The spatial differences due to bioactivity is also visible in temporal patterns. Figure 3.7 shows a Hovmöller diagram with averaged $\Delta^{17}O$ values over all longitudes up to a height of 1 km. Clearly during summer months in the northern hemisphere, values drop in the mid-latitudes due to increased assimilation. The decrease in $\Delta^{17}O$ affects lower latitudes as well by convection of air into these regions. Around the tropics in the southern hemisphere values likewise decrease due to higher bioactivity between February and June. In the year 2011 southern hemispheric $\Delta^{17}O$ values are higher than the year thereafter as a result of less interhemispheric transport from the northern to the southern hemisphere.
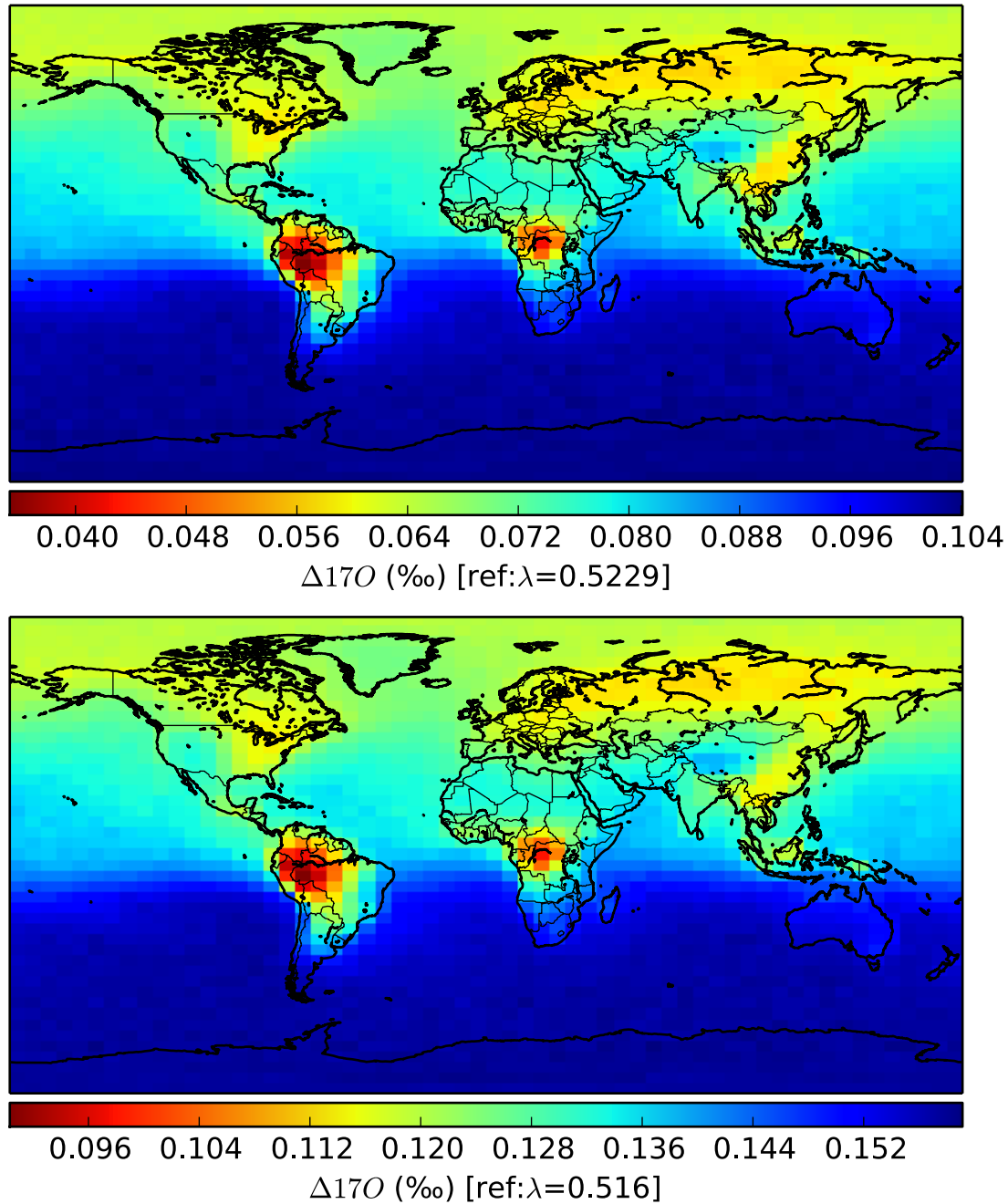
Figure 3.5: Global abundance of $\Delta^{17}O$ for the model from Hofmann (2012) at the top and Hoag et al. (2005) at the bottom averaged over 4 vertical surface layers. Note that the reference systems are kept as in the original work

Since GPP strongly determines the isotopic composition of CO_2, different $\Delta^{17}O$ abundances are expected over different ecosystems. Figure 3.8 shows GPP and $\Delta^{17}O$ for an area in the Amazon Rain Forest (12.5°S-3.5°N and 75.5°W-56.5°W) and the Canadian Tundra (60.5°N-74.5°N and 140.5°W-91.5°W). Whereas in the Amazon, $\Delta^{17}O$ shows daily and seasonal variations, signals simulated in the tundra are determined through seasonal variations. The boundary layer of the high northern latitudes in shallow, leading to a well mixed atmosphere and small day-to-day variations. The dominant
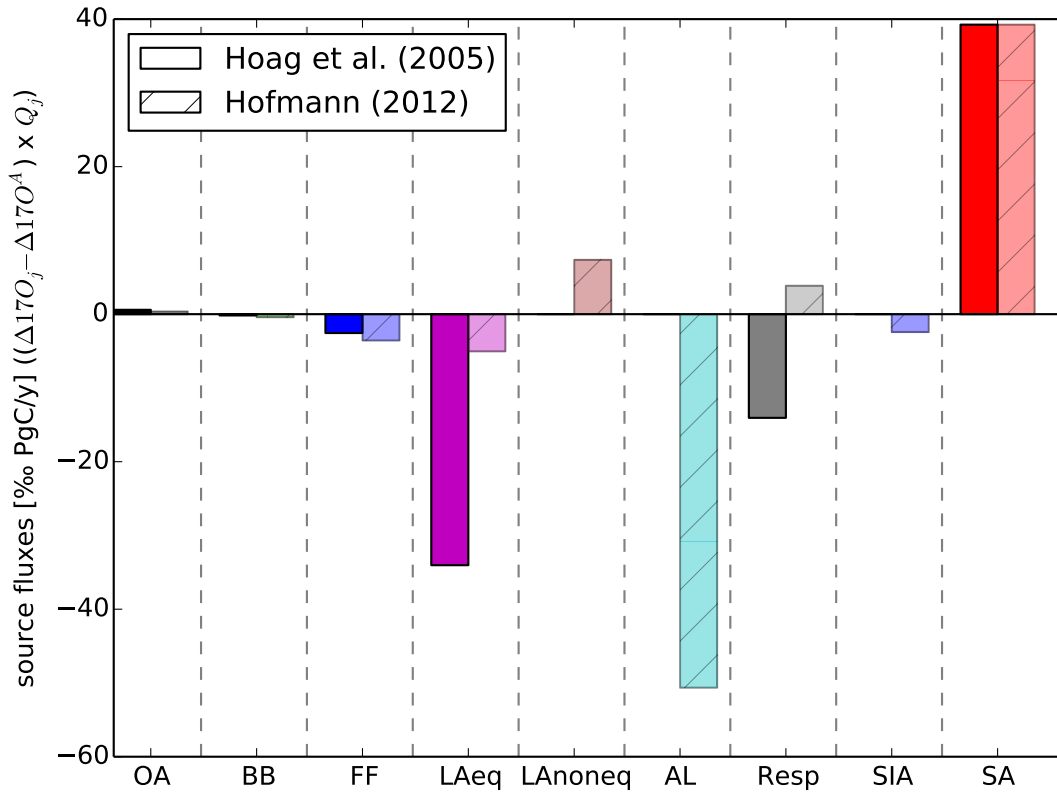
Figure 3.6: Isofluxes in ‰PgC/yr for both studies. Solid bars (1st of a pair) are according to Hoag et al. (2005), transparent bars (2nd of a pair and striped) represents the fluxes of Hofmann (2012). OA=Ocean-Atmosphere, BB=biomass burning, FF=fossil fuel, LAeq= Leaf-Atmosphere equilibrated, LAnoneq= Leaf-Atmosphere non equilibrated, AL= Atmosphere-Leaf, Resp= Rspiration, SIA= Soil-Atmosphere from Soil Invasion, SA= Stratosphere-Atmosphere

carbon flux in the latter region is the exchange with the biosphere. The influence of convection of depleted air from other regions is small due to the separation of the large scale polar cell from the mid latitudes. Therefore, the changes in $\Delta^{17}O$ are due to bioactivity and strongly follow variations in GPP. The correlation coefficient for weekly averages between GPP and $\Delta^{17}O$ is about -0.47. $\Delta^{17}O$ signals simulated for the Amazon do not show a variability as large as for the Tundra, although changes in GPP are similar between the two ecosystems. In the Amazon region, biomass burning and convection of air from the northern hemisphere contribute as well to the signal. A thorough analysis would be required to separate these counteracting effects and properly describe the impact of GPP to the signal.

The difference in $\Delta^{17}O$ values between the year 2010 and 2011 is very small as a result of similar GPP in those years for both regions. It is however known that in 2010 a severe drought caught the Amazon region thereby reducing GPP (van der Laan-Luijkx et al., 2014). SiBCASA does not account for this disturbance and it would be more appropriate to simulate with optimized carbon fluxes, which would very likely lead to larger interannual variations.
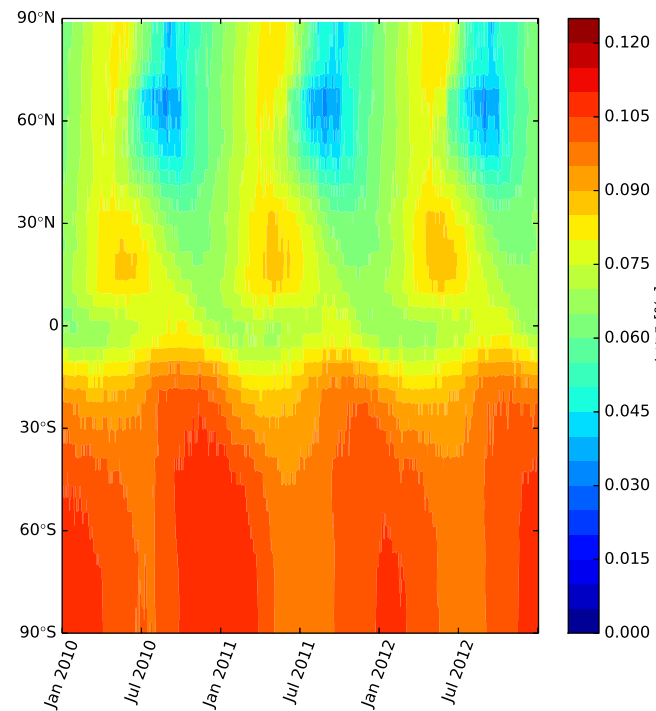
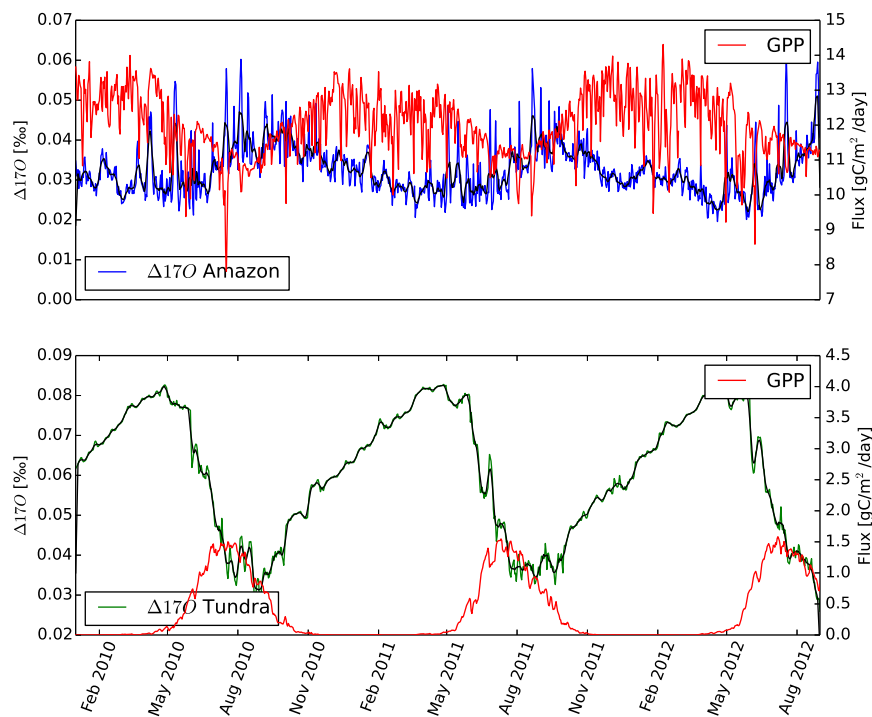**Figure 3.7:** Latitudinal band of $\Delta^{17}O$ values between 2010-2012 for the lowest kilometer

Figure 3.8: Comparison of GPP and modelled $\Delta^{17}O$ abundances between the Amazon region and the Canadian Tundra in the time period from January 2010 - September 2012 scaled per m². The black line denotes the weekly running mean

3.3   Discussion

We present the first model to simulate $\Delta^{17}O$ on a three dimensional scale to spatially and temporarily quantify the abundance of $\Delta^{17}O$. In addition, we have derived isofluxes for every grid box. This allows to simulate changes in $\Delta^{17}O$ due to assimilation and respiration, ocean, stratosphere, fossil fuel emissions and biomass burning on a high resolution from the troposphere into the stratosphere.

We have chosen to alter the $\Delta^{17}O$ values within the stratosphere in order to derive global means of $\Delta^{17}O$ that are in accordance with the box models from Hoag et al. (2005) and Hofmann (2012). Since the derived isofluxes are still too small, this approach needs to be revised. The following step would thus be to quantify the source of non-mass dependent enrichment of ^{17}O and ^{18}O in CO_2 within the stratosphere. That involves describing the photolytic oxidation of ozone and the subsequent production of $O\left(^1D\right)$. Subsequently, the transfer to $O\left(^1D\right)$ to CO_2 forming an intermediate complex, which dissociates into CO_2 and O needs to be quantified in order to determine the $\Delta^{17}O$ abundance Yung et al. (1991). At this stage, it can be said that the missing contribution of the stratospheric source globally, is compensated by very small isofluxes due to the ocean sink. Overall the chosen approach is therefore reasonable, however we need to describe both terms more thoroughly in the future.

Simulations with TM5 show a great dependency of $\Delta^{17}O$ on the biosphere. Higher bioactivity leads to smaller values in $\Delta^{17}O$. Additionally, seasonal variations can be observed in local and global means. Both results support the hypothesis by Hoag et al. (2005) that $\Delta^{17}O$ can be a measure for gross primary productivity. For both the Amazon and the Tundra, we observe that when GPP starts declining, the signal in $\Delta^{17}O$ also remains declining. The sinks of $\Delta^{17}O$ still dominate the stratospheric source. Also, atmospheric mixing and vertical transport can result in the transport of $\Delta^{17}O$ from other locations into the simulated area, leading to small $\Delta^{17}O$ abundances. It needs to be noted that the gross primary fluxes used from SiBCASA do not represent carbon fluxes for every location very well. Especially for ecosystems like the Amazon, it would be necessary to update the gross fluxes to better capture disturbances like droughts.

Despite the fact that global abundances of $\Delta^{17}O$ are in good agreement with literature, we cannot draw any conclusion yet on the accuracy of the model for distinct regions. It is therefore indispensable to compare the model output to field measurements. In the following chapter we describe the comparison to $\Delta^{17}O$ measurements taken in Göttingen (Germany) during a time period between 2010-2012.

Chapter 4

Comparison with measurements

The new gained framework of TM5 enables to study the abundance of $\Delta^{17}O$ for distinct regions and explain measurements that have been taken at a selected location. The only data set of tropospheric $\Delta^{17}O$ measured over Europe has been taken between 2010-2012 in Göttingen, Germany (Hofmann, 2012). The analysis of the measurements is however still incomplete as a 3D model was needed to explain the seasonal variations that the measurements show. In this chapter we therefore focus on the comparison of the 3D model TM5 with the measurements. It compares the seasonality in measurements and simulations and evaluates the contribution of stratospheric influx and tropospheric sinks (biosphere and fossil fuel emissions) to the $\Delta^{17}O$ abundance for the location of Göttingen. If $\Delta^{17}O$ was indeed a tracer for bioactivity (Hoag et al., 2005; Hofmann et al., 2012; Thiemens et al., 2014) then the measured and simulated signal should -even in a rural area- still depend on the activity of vegetation.

4.1 Methods

The measurements have been taken between June 2010 and July 2012 about twice per month in Göttingen (130.000 inhabitants), Germany. Air was collected around midday on top of the university building in a time frame of approximately 10 minutes The CO_2 and N_2O concentrations as well as $\delta^{18}O$ and $\delta^{17}O$ in CO_2 were measured. The measurement procedure and subsequent analysis can be found in Hofmann (2012).

We change the model set-up slightly in comparison to the previous chapter: We only use the version from Hofmann (2012), since their reference system is the same as currently cited in literature (Barkan and Luz, 2012; Thiemens et al., 2014) and since it takes fractionation through diffusion as well as equilibration into account. The model is fed with three-hourly gross fluxes for the biosphere from SiBCASA. It is run from 2001 onward until steady state in 2009. The $\Delta^{17}O$ fields for every grid box simulated on January 1st 2009 are stored. For all the runs performed in this analysis, the model is started from January 1st 2009, with the corresponding $\Delta^{17}O$ fields and CO_2 fields from December 27th, 2008. Output is stored three hourly. All figures are obtained by averaging the lowest kilometer for the region around Göttingen (49.5°-53.5° N and 7.5°-10.5° E).

We apply linear detrending to both the measurements and simulations since it separates the intra-annual changes from annual changes. The simulations are done by individually turning sinks and sources on, the calculation of isofluxes is made dependent on a constant tropospheric $\Delta^{17}O$ value of

0.06 ‰. However as the model starts with a $\Delta^{17}O$ field from 2009, the simulation time is too short to reach a new steady state if only one subroutine is turned on. Linear detrending is therefore necessary to remove the trend due to the not reached steady-state. The measurements show large inter-annual variations, and the second year is on average -0.09 ‰ lower in $\Delta^{17}O$ than the first year (see figure 4.1). This inter-annual variation cannot be explained through the model (see result and discussion section), and thus the reason for the low $\Delta^{17}O$ values in the second year is not known. It may be related either to some local effects not captured in the model or to an analytical artifact (this will be reviewed in the discussion section). In order to focus on intra-annual variations, we also apply linear detrending to the measurement data.

4.2   Results

Comparison between the experimental and modeled data only show little agreement (figure 4.1). Simulations have reached a steady state and values fluctuate around 0.060 ‰ ± 0.006 ‰ (1σ standard deviation, n=974). The measurements in return show a large difference between the first and second year of data. The average for the period June 2010-July 2011 is -0.02 ‰ ± 0.05 ‰ (1σ standard deviation, n=24), for the period August 2011-August 2012 -0.12 ‰ ± 0.04 ‰ (1σ standard deviation, n=26).
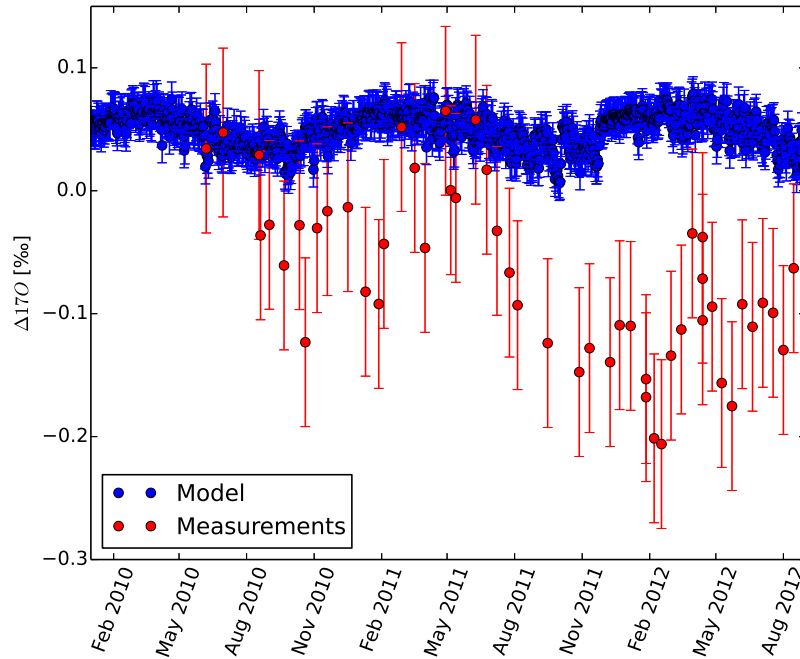

Figure 4.1: Simulations (blue) and measurements (red) for the location of Göttingen. Error bars indicate the 1σ standard deviation.

The model is not able to explain the low values, especially in the second year. Therefore, we decide to focus the following analysis on intra-annual variations.

Linearly detrended simulated and measured signals show good agreement within the 1σ standard deviation for most of the period. Figure 4.2 shows the original measurements together with their detrended and smoothed correspondences. Disagreement can be found at the beginning of 2011 and

2012 as well as in the summer months for both years. Both data sets show a strong seasonal cycle with more negative values at the end of the summer, when bioactivity is high. The lowest values for the simulations are reached on September 22nd 2010 and September 19th 2011. The smoothed measurements have their lowest values on Oct 14th 2010 and Oct 16th 2011. The amplitude for simulations is 47 per meg in 2011 and 43 per meg in 2012, with the highest values for both years on March 29th. The measurements show an amplitude of 105 per meg (in 2010), the maximum being on July 9th, and 144 per meg (in 2011) and the maximum on June 10th. The measurements show an increase in $\Delta^{17}O$ until June in both years, although vegetation is long active by that time and a decrease in $\Delta^{17}O$ would be expected. Most likely this behaviour is linked to stratospheric activity.

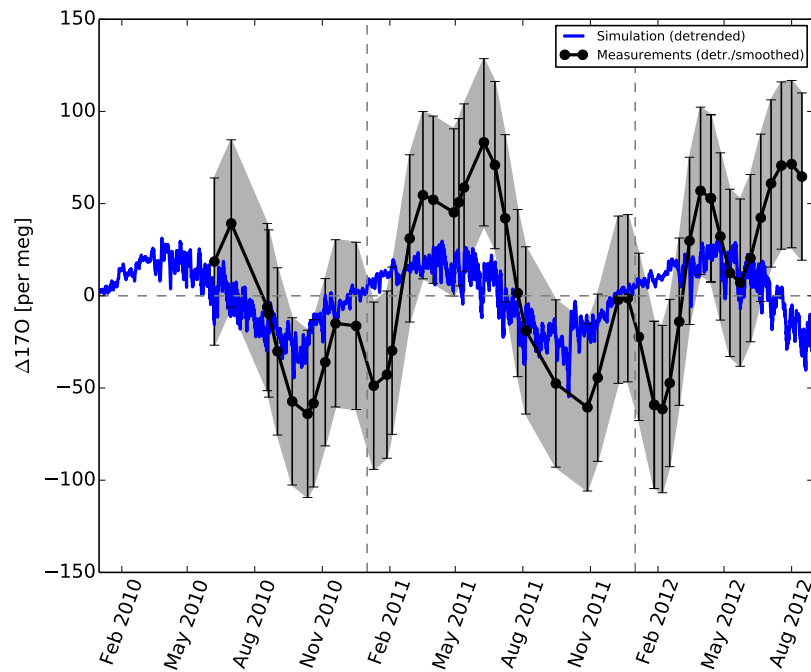**Figure 4.2:** Linearly detrended simulation (blue) and linearly detrended and smoothed measurements (black dots). Error bars indicate the 1σ standard deviation.

Individual runs of sinks and sources reveal that the seasonality in simulated signals depends mostly on biospheric activity, which can be seen in figure 4.3. Contribution from the stratosphere to the seasonal signal is low. Fossil fuel emissions alter only slightly the simulated signal in the winter months, when large anthropogenic emissions decrease the abundance of $\Delta^{17}O$. The daily variations in simulations are due to variability in biospheric activity as well as variations in the atmospheric boundary layer height. The latter impact can be seen in the day-to-day variations of fossil fuel contributions since constant monthly gross fluxes are fed into the model. The intra-monthly variations in measurements fall within the 1σ standard deviation.
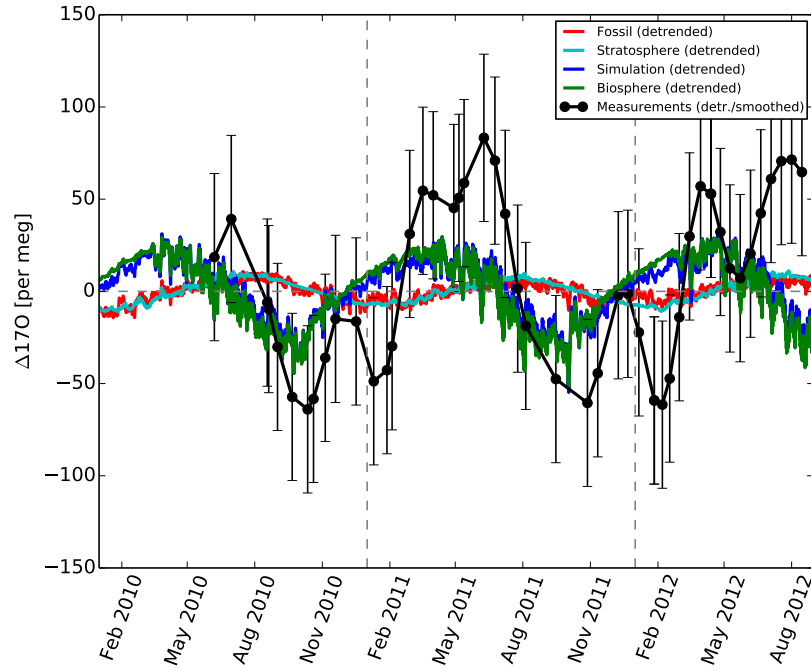
Figure 4.3: Linearly detrended $\Delta^{17}O$ values for a simulation with all sinks and sources (blue), only fossil fuel (red), only biosphere (green), only stratosphere (cyan) and smoothed and detrended measurements (black dots)

The modeled isofluxes at the location of Göttingen show a large contribution from the biosphere, followed by fossil fuel emissions (figure 4.4). Since the model output peaks earlier than the measurements, the signal could be shifted towards later times by altering the isofluxes that lead to the early peak, such as the equilibrated leaf-atmosphere flux. This can be achieved through an increase in the isotope signature of leaf water as a result of lower humidity above Göttingen.
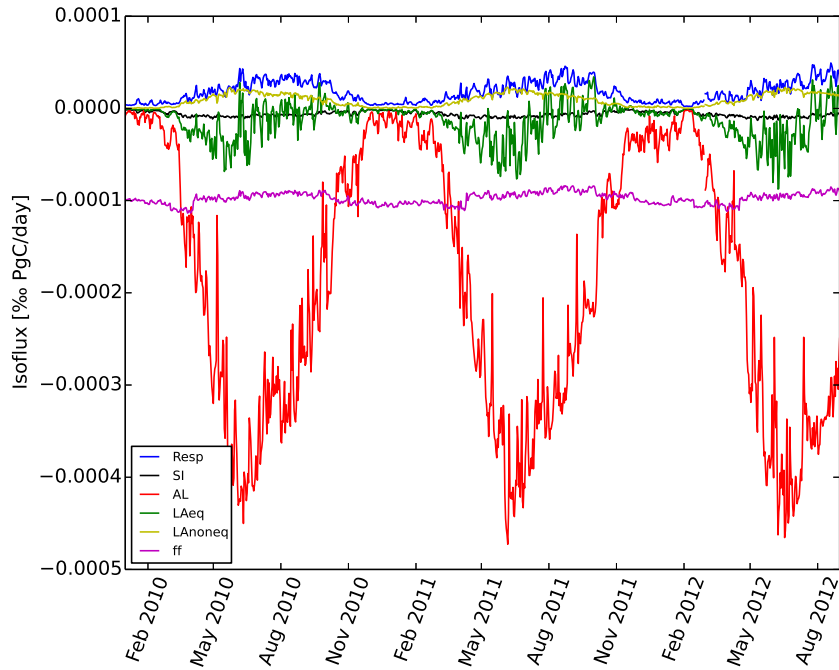
Figure 4.4: Isofluxes for Göttingen derived from the model output. Resp=Respiration isoflux, SI=soil invasion isoflux, AL=atmosphere-leaf isoflux, LAeq=leaf-atmosphere equilibrium isoflux, LAnoneq= leaf-atmosphere non-equilibrated isoflux, ff=fossil fuel isoflux

The effect of changing the leaf water isotope signature from $\Delta_L^{17} = -0.07‰$ to $\Delta_L^{17} = -0.05‰$ results in a phase shift of about three days and a decrease in amplitude of 6 per meg (shown in figure 4.5). The change would correspond to a decrease of relative humidity to 0.48, assuming that the isotopic composition of soil water is well represented. Therefore, modification of the leaf water isotope signature does not have a large effect on the simulated signals and cannot be the origin of too early peaks. In addition, a decrease in leaf water isotope signature reduces the amplitude, worsening the comparison between model and simulations.

For the winter months, very high CO_2 mole fractions were measured in Göttingen (see Appendix A.3, figure 3). For the same time period, TM5 simulates lower CO_2 mole fractions. If the high measured mixing ratios were solemnly due to large fossil fuel emissions, then the hypothesis would be that the amplitude in measurements would have been lower if these high mixing ratios had not been present. This would reduce the differences in amplitudes between the measurements and the simulation. The effect on the measured $\Delta^{17}O$ abundance, which this hypothesis would bring with it, is calculated. Figure 4.5 shows the values how the measurements should look like if the excess in CO_2 was due to fossil fuel emissions and if this excess in CO_2 was neglected. Thereby it is assumed that the modeled and measured CO_2 mole fractions are the same.

The effect of high measured CO_2 mole fractions in comparison to the simulated ones, when being solemnly due to anthropogenic emissions, cannot account for the discrepancies between simulated and modeled values.
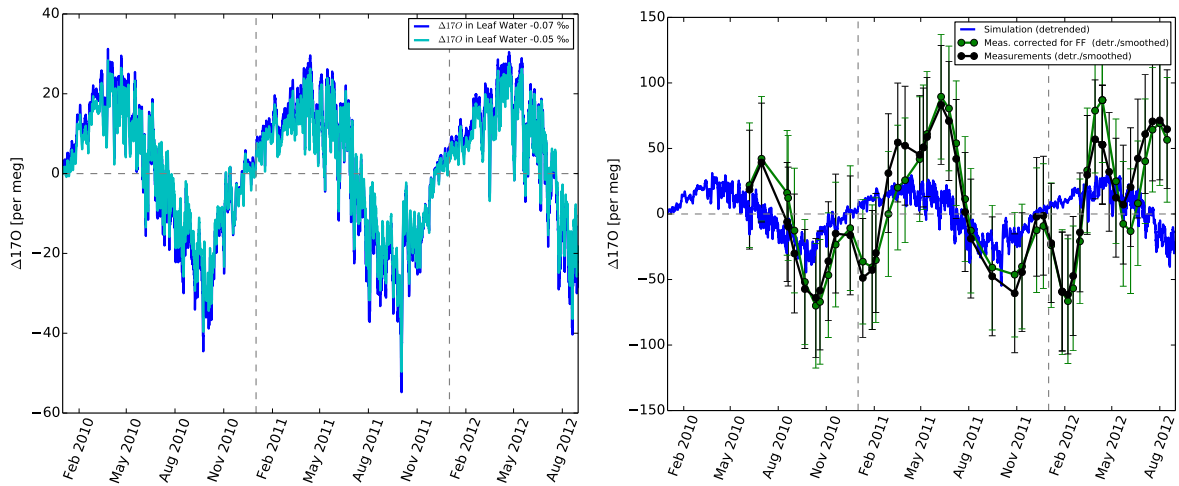
Figure 4.5: Left: Changing the isotope signature of leaf water from $-0.07\,‰$ (blue) to $-0.05\,‰$ (cyan). Right: Measurements adjusted by assuming that differences in measured and modeled CO_2 emissions are due to fossil fuel emissions (green), detrended and smoothed measurements only (black) and simulation (blue). The leaf water isotope signature is $-0.07\,‰$

4.3 Discussion

The model results can explain well the detrended seasonal variation in $\Delta^{17}O$ in surface air in Göttingen as simulated values fall mostly within the 1σ standard deviation of the measurements. Only in February and June/July of the years 2011 and 2012, the model predicts higher (in winter) or lower (in summer) values than the experimental data, but still within the 2σ standard deviation. These differences can originate from uncertainties in the model as well as the measurements. Discrepancies could be due to the large grid box, in which gross fluxes are fed, compared to the small area of Göttingen. Locally, the fluxes from the biosphere might have a larger contribution than modeled. This effect could be reduced by applying the nested zoom algorithm and increasing the resolution to $1° \times 1°$, which is part of future work.

The large difference between the non-detrended experimental data and the model is not comprehended yet. Whereas the difference in the first year is small, and most simulated values fall within the measurement uncertainty, the experimental data shows a far lower mean value for the second year. Differences within the first year could be, next to the coarse resolution, linked to improper representation of the isotopic compositions in leaf and soil-water. The effect in $\Delta^{17}O$ on assimilation and respiration has not been measured so far. This has to be done in the future by performing lab experiments. Though, the assumptions for $\Delta^{17}O$ are in accordance with assumptions on $\delta^{17}O/\delta^{18}O$ fractionation (Hofmann, 2012). Differences in the second year remain unclear. Possibly they could be related to some analytic artifacts.

The modeled $\Delta^{17}O$ values of Göttingen are $0.060\,‰ \pm 0.006\,‰$ (1σ standard deviation, n=974). This is at the lower edge of the northern hemispheric values ($0.07\,‰ \pm 0.01\,‰$, 1σ standard deviation, n=974), which is in the uncertainty range of the global abundance ($0.08\,‰ \pm 0.02\,‰$, 1σ standard deviation, n=974). The values at the low edge of the global average for Göttingen are a result of large bioactivity in that region. The variations in experimental data are, according to these results, due to bioactivity and fossil fuel emissions as well as stratospheric influence are small.

The amplitude in $\Delta^{17}O$ measurements taken in Göttingen is 0.27‰ in total, with a constant intra-annual amplitude of 0.18‰ in both years, respectively. This yearly amplitude agrees with the measured amplitudes for $\Delta^{17}O$ in La Jolla, California, US (Thiemens et al., 2014). The average abundance measured in Göttingen is however smaller. Most likely, La Jolla experiences a large influence of air convected from the nearby Pacific Ocean. Over the ocean, $\Delta^{17}O$ abundances are relatively higher than over the continent. The average $\Delta^{17}O$ at La Jolla could therefore be higher than in Göttingen, which is a more continental location. The hypothesis that differences in measured $\Delta^{17}O$ over Göttingen and La Jolla are a result of their continental or maritime location, still needs to be tested.

More investigation is needed to analyze the effect of changing biospheric gross fluxes as well as isofluxes to the simulated signal. The gross flux which is most uncertain is the soil invasion flux. In this model we kept at 30 PgC/yr (Stern et al., 2001). However, Wingate et al. (2009) found that values could be as high as 450 PgC/yr, which would reduce the simulated $\Delta^{17}O$ abundances, especially in summer. This could lead to a better agreement in amplitude between the model and the measurements. Shifting the simulated measurements to later times in the year, while enhancing the amplitude could be achieved by modification of the respiration or the non-equilibrated leaf-atmosphere isoflux. Since the global abundances of both fluxes are reasonable, enhancing the resolution of the model could already alter these fluxes for the area of Göttingen.

The phase shift in $\Delta^{17}O$ abundances between the model and the measurements could, next to the biosphere, be related to the stratospheric contribution. The isoflux in the model is only 80% of the one reported by Boering et al. (2004). A higher stratospheric isoflux would shift the peak towards later times in the year. This hypothesis still needs to be tested by first implementing the formation of heavy CO_2 in the stratosphere into TM5.

Next to the measurements taken in Göttingen, three samples were taken on top of the Brocken Mountain nearby. The measured $\Delta^{17}O$ values do not differ significantly from the values derived in the city (Hofmann, 2012). Usually, measurements from a top of a mountain represent background conditions and thus this result could indicate that measurements taken in Göttingen are not much affected by local characteristics. However, although on top of a mountain, the measurements cannot be classified as taken from a background location: The Brocken mountain is about 1100m high and samples were taken during the day, when the atmospheric boundary layer is deep and vertical mixing is large. Most likely, the sampled air is thus not taken within the free troposphere.

To fully investigate the contribution of sinks and sources to the simulated signal in absolute means, it is necessary to implement individual tracers for all compartments into TM5. This allows to run all subroutines simultaneously while still analyzing the individual contributions. Thereby, isofluxes do not have to depend on a fixed atmospheric $\Delta^{17}O$ signal.

Chapter 5

Conclusions and Recommendations

In this thesis, we have presented a model to simulate $\Delta^{17}O$ on a 3D scale. In Chapter 2 we have re-built two existing versions of box models (Hoag et al., 2005; Hofmann, 2012) and compared to each other. The main difference between the two models from Hoag et al. (2005) and Hofmann (2012) is the reference system and the inclusion of kinetic fractionation in the latter one. These effects result in different global abundances in $\Delta^{17}O$. The reference system by Hofmann (2012) has been confirmed by other studies (Luz and Barkan, 2010; Barkan and Luz, 2012) to be a good choice for $\Delta^{17}O$. The idea is that equilibration of CO_2 and H_2O is the main process determining the abundance of $\Delta^{17}O$. However, to better understand the importance of kinetic verses equilibrium fractionation, it is worth to conduct laboratory experiments. The work could include chamber experiments with labeled leaf-water to separate the contribution of equilibration (in contrast to diffusion) to the signal. Since many different scales are involved in the lifecycle of $\Delta^{17}O$ a better understanding of the effects of fractionation on $\Delta^{17}O$ will enhance our knowledge on parametrizations for small scale processes. Thereby the coupling between large scale transport and small scale changes of $\Delta^{17}O$ can be improved.

In Chapter 3 we have extended the transport model TM5 by implementing sinks and sources of $\Delta^{17}O$. The model is unique as it is the first one to simulate $\Delta^{17}O$ on a three-dimensional scale. The global abundances agree with the presented box models. At this stage we can only say that local abundances follow the patterns expected from literature. However, since there are hardly any tropospheric measurements of $\Delta^{17}O$ available, no validation has been made yet. For validation it is necessary to take measurements of tropospheric $\Delta^{17}O$ from background locations. Such a background location could be on top of a high mountain, where air can be collected from the free troposphere.

The results indicate that biospheric activity strongly influences the seasonal signal of $\Delta^{17}O$. Bioactivity is consequently also the reason for large gradients in the troposphere. These gradients exist in space and time: Areas with large bioactivity show low $\Delta^{17}O$ abundances, resulting in gradients between ecosystems and the two hemispheres. Throughout the year, $\Delta^{17}O$ abundances follow bioactivity, resulting in gradients within ecosystems. This work confirms the hypothesis of various studies, e.g. Luz et al. (1999), Hoag et al. (2005) or Hofmann (2012), that $\Delta^{17}O$ is a tracer for bioactivity. The tracer $\Delta^{17}O$ is, however, also dependent on other sinks than the biosphere, which makes the interpretation of measurements difficult. It is thus indispensable to have a good, representative model to explain and trace back the contributions to $\Delta^{17}O$ measurements. We have laid the first step towards a tool like that in this thesis. The derived model will serve as a base for further research on $\Delta^{17}O$.

Especially the analysis of simulated $\Delta^{17}O$ abundances in the Amazon rain forest indicates that yearly amplitudes in $\Delta^{17}O$ abundances may be relatively small and that day-to-day variations can be large.

This means that the measurement uncertainty could play a crucial role in explaining seasonal variations from measurements. Currently, the method from Barkan and Luz (2012) promises a high precision of 5 per meg. According to the simulated abundances over the Amazon, such a precision would be needed to see seasonal and even weekly variations. We suggest using the same reference system for all measurements to assure that comparison is easy. The newest and most promising reference system is described by Barkan and Luz (2012).

For determining GPP from measurements, the analysis of the Amazon rain forest and the Canadian Tundra suggest to measure $\Delta^{17}O$ in a remote location. It is best to choose a place where effects of anthropogenic emissions are small and where large gradients in $\Delta^{17}O$ are expected throughout the year. These large temporal gradients are needed to see seasonal variations, taking into account that the measurement uncertainty is minimal 5 per meg. The measurements taken should be representative for a large area and not biased by local characteristics. It is therefore necessary to collect samples high enough above the canopies, i.e. by aircraft or on a tower. Alternatively, measurements could be taken at different locations close to each other within the canopy and afterwards averaged. The averaged measurements will give a better representation of the larger area. The measurement frequency depends on the location. In regions with strong seasonal gradients, frequencies should be enhanced during the beginning of the growing season and reduced in periods of low activity. In regions with small seasonal variations, measurements about twice per month should be sufficient. At the same time, it may be worth to measure at a background location, i.e. on top of a mountain, to verify the model accuracy. This model will not only help to scale up point measurements to ecosystem GPP, but also to distinguish the measured signals from the biosphere to those from for example biomass burning and fossil fuel emissions.

In Chapter 4 we have used the model to explain variations in measured $\Delta^{17}O$ abundances taken in Göttingen. The modeled seasonal variations agree mostly well with the seasonality in measured signals. Seasonal variations in the measurements are due to variations in bioactivity. The weekly variations fall within the 1σ standard deviation. The model delivers at the moment a better representation for an average ecosystem, because the resolution is coarse and cannot hold for distinct locations. The discrepancies of the non-detrended simulations and original measurements in Göttingen indicate that explaining measurements is a challenge, since the scales being involved differ a lot (point measurements vs. large grid boxes). In order to better be able to combine these scales in the future, it is worth to set up a good measurement strategy: This should involve to pick a location in which very local influences can be excluded, i.e. not within a city with high fossil fuel emissions, not within a canopy. In addition the model resolution should be increased to $1° \times 1°$.

The following recommendations serve to improve the model accuracy and to build up a more detailed framework for further analysis of the tracer $\Delta^{17}O$. We list them in the order of importance:

- Characterize the isotopic composition of the stratosphere by implementing the production of enriched CO_2. This requires to implement the production of ozone and subsequent photolytic reaction to transfer the heavy oxygen molecules to CO_2.

- Implement gross ocean fluxes, instead of net fluxes, to obtain a larger isoflux. This step is certainly necessary if the stratospheric isoflux increases, as a result of the previous recommendation.

- Implement tracers for all sinks and sources. Then the contribution of each sink and source to the $\Delta^{17}O$ signal can be determined while running all subroutines simultaneously.

- More measurements of tropospheric $\Delta^{17}O$ especially for background locations are needed to validate the model. The background location should preferably be on top of a mountain and samples should be taken during the night to diminish the effect of a deep atmospheric boundary layer, ensuring to take air from the free troposphere. Preferably, the mountain is located in a more isolated place at/in the sea (i.e. Mauna Loa) such that continental effects are low.

- The resolution of the model should be increased for Göttingen in order to further analyze the discrepancy between the model and the measurements.

- Conduct laboratory experiments to characterize the effect of assimilation and respiration on $\Delta^{17}O$. Thereby the effect of equilibration verses kinetic fractionation can be further quantified.

- Use optimized carbon fluxes for gross fluxes, for regions with large inter annual variability in carbon exchange. This will result in larger inter annual gradients. This step delivers the base to analyze the distribution of $\Delta^{17}O$ as a result of disturbances in ecosystems, such as droughts.

- The model can be made even more explicit by inserting relative humidity for all grid boxes in order to calculate the isotope signature of leaf-water.

Bibliography

Appenzeller, C., Holton, J. R., and Rosenlof, K. H. (1996). Seasonal variation of mass transport across the tropopause. *Journal of Geophysical Research: Atmospheres*, 101(D10):15071–15078.

Barkan, E. and Luz, B. (2012). High-precision measurements of $^{17}O/^{16}O$ and $^{18}O/^{16}O$ ratios in CO_2. *Rapid Communications in Mass Spectrometry*, 26(23):2733–2738.

Beer, C., Reichstein, M., Tomelleri, E., Ciais, P., Jung, M., Carvalhais, N., Rödenbeck, C., Arain, M. A., Baldocchi, D., Bonan, G. B., Bondeau, A., Cescatti, A., Lasslop, G., Lindroth, A., Lomas, M., Luyssaert, S., Margolis, H., Oleson, K. W., Roupsard, O., Veenendaal, E., Viovy, N., Williams, C., Woodward, F. I., and Papale, D. (2010). Terrestrial gross carbon dioxide uptake: Global distribution and covariation with climate. *Science*, 329(5993):834–838.

Boering, K. A., Jackson, T., Hoag, K. J., Cole, A. S., Perri, M. J., Thiemens, M., and Atlas, E. (2004). Observations of the anomalous oxygen isotopic composition of carbon dioxide in the lower stratosphere and the flux of the anomaly to the troposphere. *Geophysical Research Letters*, 31(3).

Bond-Lamberty, B. and Thomson, A. (2010). Temperature-associated increases in the global soil respiration record. *Nature*, 464(7288):579–582.

Bowling, D. R., Pataki, D. E., and Randerson, J. T. (2008). Carbon isotopes in terrestrial ecosystem pools and CO_2 fluxes. *New Phytologist*, 178(1):24–40.

Bunce, J. (2005). What is the usual internal carbon dioxide concentration in C_4 species under midday field conditions? *Photosynthetica*, 43(4):603–608.

Canadell, J. G., Le Qur, C., Raupach, M. R., Field, C. B., Buitenhuis, E. T., Ciais, P., Conway, T. J., Gillett, N. P., Houghton, R. A., and Marland, G. (2007). Contributions to accelerating atmospheric CO_2 growth from economic activity, carbon intensity, and efficiency of natural sinks. *Proceedings of the National Academy of Sciences*, 104(47):18866–18870.

Ciais, P., Denning, A. S., Tans, P. P., Berry, J. A., Randall, D. A., Collatz, G. J., Sellers, P. J., White, J. W. C., Trolier, M., Meijer, H. A. J., Francey, R. J., Monfray, P., and Heimann, M. (1997). A three-dimensional synthesis study of ^{18}O in atmospheric CO_2: 1. surface fluxes. *Journal of Geophysical Research: Atmospheres*, 102(D5):5857–5872.

Cox, P. M., Betts, R. A., Jones, C. D., Spall, S. A., and Totterdell, I. J. (2000). Acceleration of global warming due to carbon-cycle feedbacks in a coupled climate model. *Letters to Nature*, 408(6809):184–187.

Cramer, W., Kicklighter, D. W., Bondeau, A., Iii, B. M., Churkina, G., Nemry, B., Ruimy, A., Schloss, A. L., and Intercomparison, T. P. O. T. P. N. M. (1999). Comparing global models of terrestrial net primary productivity (NPP): overview and key results. *Global Change Biology*, 5(S1):1–15.

Dee, D. P., Uppala, S. M., Simmons, A. J., Berrisford, P., Poli, P., Kobayashi, S., Andrae, U., Bal-maseda, M. A., Balsamo, G., Bauer, P., Bechtold, P., Beljaars, A. C. M., van de Berg, L., Bidlot, J., Bormann, N., Delsol, C., Dragani, R., Fuentes, M., Geer, A. J., Haimberger, L., Healy, S. B., Hersbach, H., Hlm, E. V., Isaksen, L., Kllberg, P., Khler, M., Matricardi, M., McNally, A. P., Monge-Sanz, B. M., Morcrette, J.-J., Park, B.-K., Peubey, C., de Rosnay, P., Tavolato, C., Thpaut, J.-N., and Vitart, F. (2011). The ERA-interim reanalysis: configuration and performance of the data assimilation system. *Quarterly Journal of the Royal Meteorological Society*, 137(656):553–597.

Ehleringer, J. R., Bowling, D. R., Flanagan, L. B., Fessenden, J., Helliker, B., Martinelli, L. A., and Ometto, J. P. (2002). Stable isotopes and carbon cycle processes in forests and grasslands. *Plant Biology*, 4(2):181–189.

Eiler, J. and Schauble, E. (2004). $^{18}O\,^{13}C\,^{16}O$ in earths atmosphere. *Geochimica et Cosmochimica Acta*, 68(23):4767–4777.

Farquhar, K., J., L., Taylor, J., Flanagan, L. B., Syvertsen, J., Hubik, K., Wong, C. S., and Ehleringer, J. R. (1993). Vegetation effects on the isotope composition of oxygen in in atmospheric CO_2. *Nature*, 363(6428):439–443.

Francey, R. J. and Tans, P. P. (1987). Latitudinal variation in oxygen-18 of atmospheric CO_2. *Nature*, 327(6122):495–497.

Giglio, L., Randerson, J. T., and van der Werf, G. R. (2013). Analysis of daily, monthly, and annual burned area using the fourth-generation global fire emissions database (GFED4). *Journal of Geophysical Research: Biogeosciences*, 118(1):317–328.

Gillon, J. S. and Yakir, D. (2000). Naturally low carbonic anhydrase activity in C_4 and C_3 plants limits discrimination against $C^{18}OO$ during photosynthesis. *Plant, Cell & Environment*, 23(9):903–915.

Gilmanov, T. G., Verma, S. B., Sims, P. L., Meyers, T. P., Bradford, J. A., Burba, G. G., and Suyker, A. E. (2003). Gross primary production and light response parameters of four southern plains ecosystems estimated using long-term CO_2-flux tower measurements. *Global Biogeochemical Cycles*, 17(2).

Hoag, K. J., Still, C. J., Fung, I. Y., and Boering, K. A. (2005). Triple oxygen isotope composition of tropospheric carbon dioxide as a tracer of terrestrial gross carbon fluxes. *Geophysical Research Letters*, 32(2).

Hofmann, M. E., Horvth, B., and Pack, A. (2012). Triple oxygen isotope equilibrium fractionation between carbon dioxide and water. *Earth and Planetary Science Letters*, 319320(0):159 – 164.

Hofmann, M. E. G. (2012). *Triple oxygen isotope variations in natural and anthropogenic carbon dioxide*. PhD thesis, Georg-August-Universität Göttingen.

Holtslag, A. A. M. and Boville, B. A. (1993). Local versus nonlocal boundary-layer diffusion in a global climate model. *Journal of Climate*.

Horváth, B., Hofmann, M., and Pack, A. (2012). On the triple oxygen isotope composition of carbon dioxide from some combustion processes. *Geochimica et Cosmochimica Acta*, 95(0):160–168.

Huijnen, V., Williams, J., van Weele, M., van Noije, T., Krol, M., Dentener, F., Segers, A., Houweling, S., Peters, W., de Laat, J., Boersma, F., Bergamaschi, P., van Velthoven, P., Le Sager, P., Eskes, H., Alkemade, F., Scheele, R., Nédélec, P., and Pätz, H.-W. (2010). The global chemistry transport

model TM5: description and evaluation of the tropospheric chemistry version 3.0. *Geoscientific Model Development*, 3(2):445–473.

Hulston, J. R. and Thode, H. G. (1965). Variations in the s33, s34, and s36 contents of meteorites and their relation to chemical and nuclear effects. *Journal of Geophysical Research*, 70(14):3475–3484.

IPCC (2013). *IPCC, 2013: Climate Change 2013: The Physical Science Basis. Contribution of Working Group I to the Fifth Assessment Report of the Intergovernmental Panel on Climate Change.* Cambridge University Press, Cambridge, United Kingdom and New York, NY, USA.

Jacobson, A. R., Mikaloff Fletcher, S. E., Gruber, N., Sarmiento, J. L., and Gloor, M. (2007). A joint atmosphere-ocean inversion for surface fluxes of carbon dioxide: 1. methods and global-scale fluxes. *Global Biogeochemical Cycles*, 21(1).

Krol, M., Houweling, S., Bregman, B., van den Broek, M., Segers, A., van Velthoven, P., Peters, W., Dentener, F., and Bergamaschi, P. (2005). The two-way nested global chemistry-transport zoom model TM5: algorithm and applications. *Atmospheric Chemistry and Physics*, 5(2):417–432.

Lämmerzahl, P., Röckmann, T., Brenninkmeijer, C. A. M., Krankowsky, D., and Mauersberger, K. (2002). Oxygen isotope composition of stratospheric carbon dioxide. *Geophysical Research Letters*, 29(12):23–1–23–4.

Le Quéré, C., Raupach, M. R., Canadell, J. G., and Marland et al., G. (2009). Trends in the sources and sinks of carbon dioxide. *Nature Geosciences*, 2(12):831–836.

Louis, J.-F. (1979). A parametric model of vertical eddy fluxes in the atmosphere. *Boundary-Layer Meteorology*, 17(2):187–202.

Luz, B. and Barkan, E. (2010). Variations of $^{17}O/^{16}O$ and $^{18}O/^{16}O$ in meteoric waters. *Geochimica et Cosmochimica Acta*, 74(22):6276 – 6286.

Luz, B., Barkan, E., Bender, M., Thiemens, M., and Boering, K. A. (1999). Triple-isotope composition of atmospheric oxygen as a tracer of biosphere productivity. *Letter to Nature*, 400:547–550.

Marland, G., Boden, T., and Andres, R. (2003). *Trends: A Compendium of Data on Global Change*. Carbon Dioxide Information Analysis Center, Environmental Sciences Division, Oak Ridge National Laboratory, Oak Ridge, Tennessee.

Pearcy, R. W. and Ehleringer, J. R. (1984). Comparative ecophysiology of C_3 and C_4 plants. *Plant, Cell and Environment*, 7(1):1–13.

Potter, C. S., Randerson, T., Field, C., Matson, P., Vitousek, P., Mooney, H., and Klooster, S. (1993). Terrestrial ecosystem production: A process-oriented model based on global satellite and surface data. *Global Biogeochemical Cycles*, 7(4):811–841.

Russell, G. L. and Lerner, J. A. (1981). A new finite-differencing scheme for the tracer transport equation. *Journal of Applied Meteorology*.

Schaefer, K., Collatz, G. J., Tans, P., Denning, A. S., Baker, I., Berry, J., Prihodko, L., Suits, N., and Philpott, A. (2008). Combined simple biosphere/carnegie-ames-stanford approach terrestrial carbon cycle model. *Journal of Geophysical Research: Biogeosciences*, 113(G3).

Schimel, D. S. (1995). Terrestrial ecosystems and the carbon cycle. *Global Change Biology*, 1(1):77–91.

Schimel, D. S., House, J. I., Hibbard, K. A., Bousquet, P., Ciais, P., Peylin, P., Braswell, B. H., Apps, M. J., Baker, D., Bondeau, A., Canadell, J., Churkina, G., Cramer, W., Denning, A. S., Field, C. B., Friedlingstein, P., Goodale, C., Heimann, M., Houghton, R. A., Melillo, J. M., Moore, B., Murdiyarso, D., Noble, I., Pacala, S. W., Prentice, I. C., Raupach, M. R., Rayner, P. J., Scholes, R. J., Steffen, W. L., and Wirth, C. (2001). Recent patterns and mechanisms of carbon exchange by terrestrial ecosystems. *Nature*, 414(6860):169–172.

Stern, L. A., Amundson, R., and Baisden, W. T. (2001). Influence of soils on oxygen isotope ratio of atmospheric co2. *Global Biogeochemical Cycles*, 15(3):753–759.

Still, C. J., Berry, J. A., Collatz, G. J., and DeFries, R. S. (2003). Global distribution of C_3 and C_4 vegetation: Carbon cycle implications. *Global Biogeochemical Cycles*, 17(1):6–1–6–14.

Thiemens, M. H. (1999). Mass-independent isotope effects in planetary atmospheres and the early solar system. *Science*, 283(5400):341–345.

Thiemens, M. H., Chakraborty, S., and Jackson, T. L. (2014). Decadal $D^{17}O$ record of tropospheric CO_2: Verification of a stratospheric component in the troposphere. *Journal of Geophysical Research: Atmospheres*, 119(10):6221–6229.

van der Laan-Luijkx, I., van der Velde, I., Krol, M., Gatti, L., Miller, J., Gloor, M., van Leeuwen, T., Kaiser, J., Wiedinmyer, C., Basu, S., Clerbaux, C., and Peters, W. (2014). Response of the amazon carbon balance to the 2010 drought derived with carbontracker south america. under review.

van der Velde, I. R., Miller, J. B., Schaefer, K., Masarie, K. A., Denning, S., White, J. W. C., Tans, P. P., Krol, M. C., and Peters, W. (2013). Biosphere model simulations of interannual variability in terrestrial $^{13}C/^{12}C$ exchange. *Global Biogeochemical Cycles*, 27(3):637–649.

van der Werf, G. R., Randerson, J. T., Collatz, G. J., Giglio, L., Kasibhatla, P. S., Arellano, A. F., Olsen, S. C., and Kasischke, E. S. (2004). Continental-scale partitioning of fire emissions during the 1997 to 2001 el nio/la nia period. *Science*, 303(5654):73–76.

van der Werf, G. R., Randerson, J. T., Giglio, L., Collatz, G. J., Mu, M., Kasibhatla, P. S., Morton, D. C., DeFries, R. S., Jin, Y., and van Leeuwen, T. T. (2010). Global fire emissions and the contribution of deforestation, savanna, forest, agricultural, and peat fires (19972009). *Atmospheric Chemistry and Physics*, 10(23):11707–11735.

West, J. B., Sobek, A., and Ehleringer, J. R. (2008). A simplified GIS approach to modeling global leaf water isoscapes. *PLoS ONE*, 3(6):e2447.

Wiegel, A. A., Cole, A. S., Hoag, K. J., Atlas, E. L., Schauffler, S. M., and Boering, K. A. (2013). Unexpected variations in the triple oxygen isotope composition of stratospheric carbon dioxide. *Proceedings of the National Academy of Sciences*, 110(44):17680–17685.

Wingate, L., Oge, J., Cuntz, M., Genty, B., Reiter, I., Seibt, U., Yakir, D., Maseyk, K., Pendall, E. G., Barbour, M. M., Mortazavi, B., Burlett, R., Peylin, P., Miller, J., Mencuccini, M., Shim, J. H., Hunt, J., and Grace, J. (2009). The impact of soil microorganisms on the global budget of 18o in atmospheric co2. *Proceedings of the National Academy of Sciences*, 106(52):22411–22415.

Woodwell, G. M. and Whittaker, R. H. (1968). Primary production in terrestrial ecosystems. *American Zoologist*, 8(1):19–30.

Xiao, X., Zhang, Q., Braswell, B., Urbanski, S., Boles, S., Wofsy, S., III, B. M., and Ojima, D. (2004). Modeling gross primary production of temperate deciduous broadleaf forest using satellite images and climate data. *Remote Sensing of Environment*, 91(2):256 – 270.

Young, E. D., Galy, A., and Nagahara, H. (2002). Kinetic and equilibrium mass-dependent isotope fractionation laws in nature and their geochemical and cosmochemical significance. *Geochimica et Cosmochimica Acta*, 66(6):1095 – 1104.

Yung, Y. L., DeMore, W., and Pinto, J. P. (1991). Isotopic exchange between carbon dioxide and ozone via O(1D) in the stratosphere. *Geophysical research letters*, 18(1):13–16.

Acknowledgments

Appendix

A.1 Overview input parameters for the box-models

Table 1: Overview of the input parameters used by Hoag et al. (2005) and Hofmann (2012)

Parameter	Description	Hoag et al. (2005)	Hofmann (2012)	Unit
$\frac{dM}{dt}$	rate of increase of tropospheric CO_2	3.2	4	PgC/yr
GPP	gross primary productivity	100	120	PgC/yr
F_A	assimilation rate	88	106	PgC/yr
F_{LA}	leaf-atmosphere flux	152.5	246	PgC/yr
F_{LAeq}	equilibrated leaf-atmosphere flux	137.5	197	PgC/yr
$F_{LAnoneq}$	non-equilibrated leaf-atmosphere flux	15	49	PgC/yr
F_{AL}	atmosphere-leaf flux	-240.5	-352	PgC/yr
F_{resp}	respiration flux	82.7	103	PgC/yr
F_{SA}	stratosphere-atmosphere flux	107	100	PgC/yr
F_{AS}	atmosphere-stratosphere flux	-107	-100	PgC/yr
F_{OA}	ocean-atmosphere flux	90	90	PgC/yr
F_{AO}	atmosphere-ocean flux	-92	-92	PgC/yr
F_{SIA}	soil invasion flux (source)	0	30	PgC/yr
F_{ASI}	soil invasion flux (sink)	0	-30	PgC/yr
F_{FF}	fossil fuel flux	6	8	PgC/yr
F_{bb}	biomass burning flux	1.6	1	PgC/yr
Θ_{C_3}	degree of CO_2 equilibration in C3 plants	0.93	0.93	-
Θ_{C_4}	degree of CO_2 equilibration in C4 plants	0.38	0.38	-
f_{C3}	fraction C_3 plants	0.82	0.77	-
f_{C3}	fraction C_4 plants	0.18	0.23	-
C_c/C_a	CO_2 gradient between stomata and atmosphere	2/3 for C_3 1/3 for C_4	0.7	-
Δ_A^{17}	modeled $\Delta^{17}O$ value of atmospheric CO_2			‰
Δ_L^{17}	$\Delta^{17}O$ value of CO_2 equilibrated with leaf water	0	-0.07	‰
Δ_{SW}^{17}	$\Delta^{17}O$ value of CO_2 equilibrated with soil water	0	-0.01	‰
Δ_{resp}^{17}	$\Delta^{17}O$ value of CO_2 from respiration	0	0.08	‰
Δ_{ocean}^{17}	$\Delta^{17}O$ value of ocean water	0	-0.005	‰
$\Delta^{17}O$	$\Delta^{17}O$ value of CO_2 equilibrated with ocean water	0	-0.005	‰

Table 1 – continued from previous page

Parameter	Description	Hoag et al. (2005)	Hofmann (2012)	Unit
Δ^{17}_{strat}	$\Delta^{17}O$ value of CO_2 from stratosphere	$\Delta^{17}_A + 0.42$	$\Delta^{17}_A + 0.445$	‰
Δ^{17}_{SI}	$\Delta^{17}O$ value of CO_2 equilibrated with soil water	0	-0.01	‰
Δ^{17}_{FF}	$\Delta^{17}O$ value of CO_2 from fossil fuel combustion	-0.155	-0.32	‰
Δ^{17}_{bb}	$\Delta^{17}O$ value of CO_2 from land use change	0	-0.21	‰
$\alpha_{CO_2-water}$	$\delta^{18}O$ equilibrium fractionation factor	-	(17.604/T -0.01793)+1	-
$\theta_{CO_2-water}$	$\Delta^{17}O$ equilibrium fractionation factor	0.516	0.522	-
α_{trans}	enrichment of ^{18}O in leaf water from evapotranspiration	-	0.9917	-
λ_{trans}	$\Delta^{17}O$ equilibrium fractionation factor for transpiration	-	0.522-0.008 × h	-
h	average humidity above leaf	-	0.8	-
α_L	$\delta^{18}O$ kinetic fractionation factor for stomata diffusion	-	0.9926	-
α_s	$\delta^{18}O$ kinetic fractionation factor for soil diffusion	-	0.9928	-
λ_{kin}	$\Delta^{17}O$ factor for kinetic fractionation	-	0.509	-
λ_{RL}	slope of CO_2 -water equilibration line (reference line)	0.516	0.522	-
λ_{GMWL}	slope of global meteoric water line	-	0.528	-
γ_{GMWL}	intercept of GMWL	-	0.033	‰
T_{soil}	average soil temperature	-	285	K
T_{leaf}	average leaf temperature	-	285	K
T_{ocean}	average ocean temperature	-	291	K

44

A.2   Flux data fossil fuel emissions and biomass burning
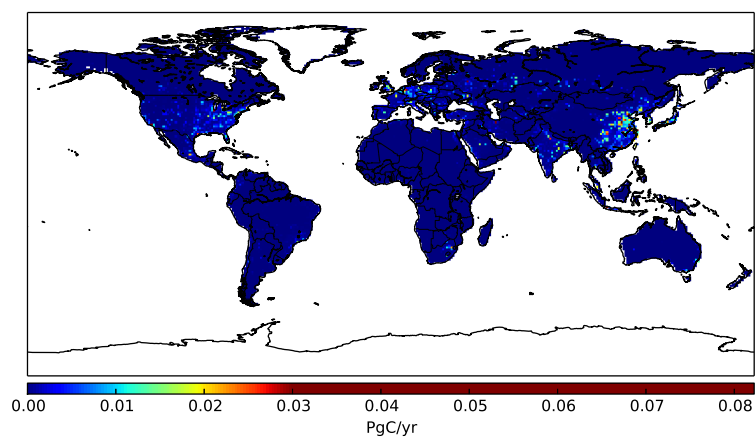

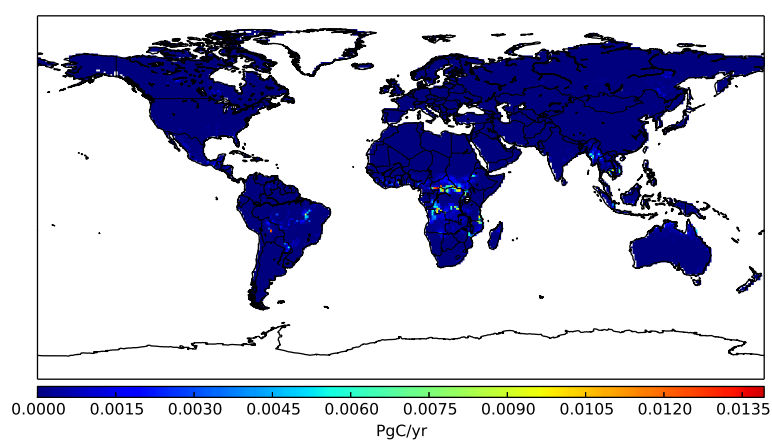**Figure 1:** Emissions from fossil fuel combustion in 2011

Figure 2: Emissions from biomass burning in 2011

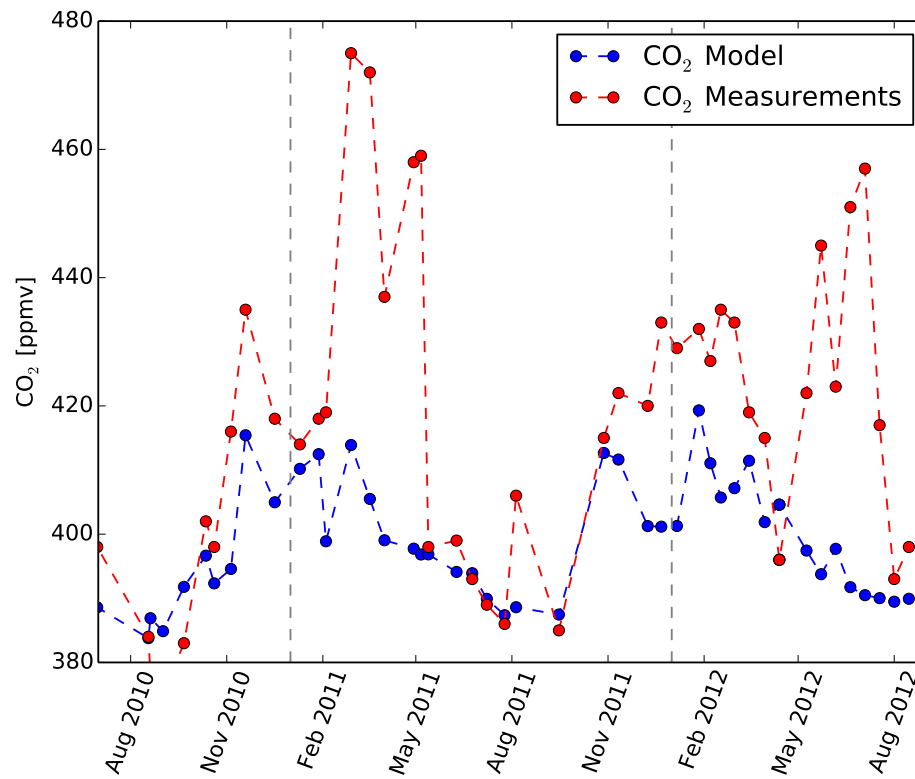## A.3   CO$_2$ data measured and simulated in Göttingen

Figure 3: Measured in Göttingen (red) and simulated (blue) CO$_2$ mole fractions for the time period August 2010-August 2012